UNIVERSITAT DE BARCELONA

Final Degree Project

Biomedical Engineering Degree

Validation of the PSIR sequence for the determination of arrhythmogenic channels in ventricular ischemia

Barcelona, 21 of January of 2022

Author: Jaime Cayetano Serrano Campaner

Director: Paz Garré Anguera de Sojo

Tutor: Paz Garré and Sara Vázquez

ACKNOWLEDGEMENT

I wish to express my deepest gratitude to several individuals without whom this undertaking would not have been possible,

First of all, I must thank my tutor, Paz Garré, for giving me the opportunity to develop the experimental part of my work in the arrhythmia unit of the Hospital Clínic, for her total involvement in the project and her constant help. Her immense knowledge has allowed me to complete this research and has taught me how to work with cardioresonance imaging using professional software. I could not have imagined having a better supervisor in my study.

Secondly, I would like to acknowledge my other tutor, Sara Vázquez, for her valuable collaboration. She has been a great support for me, a source of motivation and has always been available to solve any doubt and guide me in any part of the work.

Thirdly, I must also mention Mariona Regany, a worker in the arrhythmia unit with whom it has been a pleasure to share the work computer. I must thank her both for the interest she has shown in my study and for all the times she has made an effort to lend me the computer and allow me to progress in my work.

Also, I would like to thank all my friends and fellow biomedical engineers whom I have shared these four years of hard work and remarkable experiences. Finally, I would like to express my gratitude to my family for their unconditional support.

ABSTRACT

In patients with ventricular tachycardia of ischemic origin, arrhythmogenic channels are the pathway of abnormal tissue activation and their determination in the substrate is a essential factor when treating these cases by radiofrequency ablation.

Extracting this information from images obtained by magnetic resonance imaging has great advantages over other more invasive imaging techniques. The most commonly used reconstruction technique in MRI-2D is the Magnitude sequence. Recently, another sequence called Phase Sensitive Inversion Recovery (PSIR) is beginning to be established, which takes into account the polarity of the protons, apart from their magnitude, when generating the image.

In this project the level of validity of the PSIR reconstruction sequence to determine the arrhythmogenic channels has been demonstrated, comparing data obtained using this sequence with data obtained using the strongly validated and referenced Magnitude sequence. Data from 21 patients with specific conditions have been used for this study. The images have been segmented and processed in order to extract the parameters that have allowed to solve the question raised by means of a statistical analysis of the information obtained.

We have worked with ADAS-3D rendering software to study the cases and have determined the configuration that allows the highest quality in the visualization of PSIR images, specifically the setting of contrast thresholds.

From the information provided by the ADAS-3D we selected the information considered relevant for the statistical analysis, descriptive information about the channels and characteristics of the tissue. These data, together with the contrast thresholds set in the study, have been statistically analysed with the RStudio programme.

Valuable information has been obtained from the results. The ideal thresholds for studying PSIR images have been found and it has been concluded that there is a considerable similarity between both sequences when interpreting MRI images clinically, although not enough to validate it completely. Regarding the characterisation of channels, a high accuracy in the calculation of their mass has been determined, but a great inaccuracy in their counting. In terms of quantification, identification and classification of ventricular tissue, considerable correlation and acceptable measurement accuracy have been demonstrated.

KEYWORDS

ischemic ventricular tachycardia - arrhythmogenic channels – MRI – Magnitude sequence – PSIR sequence – ADAS-3D – segmentation – contrast thresholds

GLOSSARY OF TERMS

MRI: Magnetic Resonance Imaging

GBCA: Gadolinium-based contrast agents

MAG: Magnitude reconstruction sequence

PSIR: Phase-Sensitive Inversion Recovery reconstruction sequence

LV: Left ventricle

VT: Ventricular Tachycardia

VF: Ventricular Fibrillation

QRS: Graphic representation of the depolarization of the ventricles of the heart forming a spiky structure on the electrocardiogram.

CC: Conducting Channel. Arrhythmogenic Channel. Conducting Corridor.

BZ: Border Zone area between ischemic and healthy tissue

SD: Standard deviation

SE: Standard error

n: Sample's size

r: Pearson's product moment correlation coefficient

TABLE OF CONTENTS

1. INTRODUCTION

1.1. Objectives of the project

The main objective of this Final Degree Project is to validate the accuracy of the PSIR sequence in determining arrhythmogenic channels in patients with ischemic ventricular tachycardia.

The PSIR sequence is a reconstruction technique for generating images using 2D MRI. This technique has been established a few years ago in the health sector and has meant a considerable advance for the clinical study of a large number of pathologies that are diagnosed by MRI. The main advantage of this sequence is that it generates less artifact because it corrects the inversion time. In the case of ischemic cardiomyopathology, late gadolinium enhancement MRI is used to identify the arrhythmic substrate. The ischemic tissue is formed by three different tissues: healthy tissue, dense scar tissue and an intermediate tissue called border zone, which can conduct electricity very slow, being able to create a slow conduction channel and perpetuate a ventricular tachycardia.

The purpose of this work is to determine the validity of the PSIR reconstruction technique, using real patient data and professional software equipment, taking as a reference another already validated reconstruction sequence, the Magnitude reconstruction sequence, which has been established for years in the field. The study consists of investigating whether the efficiency of the PSIR sequence in correctly representing and interpreting ischemic ventricles (healthy zones, fibrotic zones, BZ areas and CC) is equivalent to that of the MAG sequence. This verification will be estimated by means of a study, with a suitable number of patients, comparing maps from the same patient obtained with PSIR and with MAG. Certain analysis parameters will be evaluated, such as: the number of corridors detected, their mass and position, area of each type of tissue detected. In addition, it is also intended to find and fix the appropriate contrast threshold to accurately differentiate healthy ventricular regions from ischemic ones and to correctly determine the CC in the maps formed by PSIR resonance imaging.

Once the general objectives of the project have been defined, I must break it down into several more specific objectives to guide the work until the general objective is achieved. The specific objectives for this work are the following:

- Selection of patients with the appropriate conditions for the work
- Data selection and download: 1 MAG sample and 1 PSIR sample for each patient
- Segmentation and representation of each sample by software
- Adjustment of the appropriate contrast in PSIR cases
- Selection and extraction of discriminatory features and parameters
- Comparative study
- Analysis of obtained results and conclusion

Considering all these objectives, it will be necessary to follow a work process that involves getting to know the state of the technology and the market and, from here, creating a task plan to carry out the experimental part of the project in the arrhythmia unit of the Hospital Clínic of Barcelona.

1.2. Scope of the project

DEFINITION OF SCOPE

This project is a research work with experimental demonstration; therefore, it is aimed to investigate a specific question. Although this means that at the initial stage no specific results are expected at the end of the work, it is expected to provide an answer to the question posed by the main objective of the project, that is to find out whether the PSIR sequence is completely valid and effective, as is MAG.

The reason why the project focuses on the determination of arrhythmogenic channels using the PSIR reconstruction technique is because they are a highly relevant element that is considered before and during ablation procedures, the purpose of which is to treat a wide variety of heart diseases. There is a certain degree of uncertainty, on the part of the professionals at Hospital Clínic of Barcelona, as to the efficacy and accuracy of this novel method for detecting these channels with respect to the classic MAG sequence. It is suspected that the PSIR sequence, by correcting the inversion time, apart from eliminating artifacts, may also alter some details of the gadolinium enhancement and fail to detect channels.

Therefore, the project aims to validate a very specific methodology to reduce the level of uncertainty that surrounds it. In addition, it seeks to establish and adjust contrast values that determine as accurately as possible the CC of the arrhythmia. On the other hand, it also aims to develop a research pathway in order to obtain results that can serve as a source of information for subsequent studies and thus promote progress in this field of study.

Finally, I must submit a report that explains a theoretical framework, defines the methodologies used, describes the experimental process and provides results with their respective analytical conclusions.

FIELD

Taking into account what has been said in the previous sections, it is acceptable to state that the field of this project is in the cardiac resonance sector specialized in arrhythmias. This includes companies developing cardioresonance equipment and software, centers for the diagnosis of heart disease by imaging, specialized research teams or even arrhythmia units in hospitals.

PROCEDURES AND STRUCTURE OF THE PROJECT

The development of the project will be carried out in person in an office of the arrhythmia unit of the Hospital Clínic of Barcelona. This is because the information I have worked with cannot leave the hospital for legal reasons. In addition, I have had the support of the two professionals who have tutored my work, Paz Garré and Sara Vázquez. Their collaboration has consisted of training on the use of the equipment, resolution of doubts and periodic meetings to define the direction of the project.

The resources will be limited to those provided by the hospital and the University of Barcelona. Additionally, this project should be sized for a total of 300 hours.

REQUIREMENTS

The essential requirements of the work are the following:

- Availability of valid data to perform the experimental part
- Availability of the necessary reconstruction, processing and segmentation equipment and software.
- Training on the use and operation of the equipment
- Support in image processing tasks
- Collaboration in statistical studies

LIMITATIONS

	INCLUIDED	*EXCLUDED*
INDISPENSABLE	- Correct data selection - Acquisition of PSIR and MAG MRI - Processing and segmentation - Parameter extraction - Comparison between both methods - Analysis of obtained values	- Contrast with other image acquisition methods - Contrast processing and segmentation techniques - Channel location validation
DESIRABLE	- Perform post-processing and review of segmentations - Determine the ideal contrast threshold	- Compare different contrast agents for image capture - Compare with electroanatomical maps - Improve possible accuracy error - Correct noise caused by processing using filters

Table 1: Table of project limitations.

PROJECT CONSTRAINTS AND INITIAL RISKS

This project takes approximately 300 hours to complete and is given as a student. Also, for the experimental stage it is essential to obtain real patient data. These realities result in a set of constraints and risks that limit my work in specific dimensions. The main restrictions of the work are the following:

- Time constraint that may cause accumulation of tasks.
- Lack of experience with the equipment, software and the industry in general.
- A limited number of patients suitable for the study in the database may affect the quality of the results.
- Image acquisition and segmentation processes are operator-dependent, so they can be a differentiating factor between independent images in terms of the parameters studied.
- Difficulty in finding variables that describe exactly the characteristics I want to buy, e.g. position and hazard of the channels.

2. BACKGROUND

2.1. State of the art

2.1.1. Ischemic ventricular tachycardia

The heart creates and sends electrical impulses that cause the atria to contract and, consequently, drive blood into the ventricles. Electrical signals then reach the ventricles, contracting them and pumping blood to the lungs and the rest of the body.

This electrical signal originates in the sinoatrial node, which paces the heartbeat and is located at the top of the right atrium. When this natural pacemaker generates an electrical impulse, it stimulates the atria to contract. The signal then passes through the atrioventricular node. There, the signal stops for a brief moment and then is sent through the muscle fibres of the ventricles, stimulating their contraction.

Although the sinoatrial node sends electrical impulses at a certain rate, the heart rate can vary according to physical demands, stress level or due to hormonal factors.

Starting from the beginning, it is of great relevance to explain how this heart disease affects the population. Ventricular arrhythmias contribute hugely to the morbidity and mortality of patients with coronary artery disease. Coronary artery disease is the most common type of heart disease, in fact, it is the leading cause of death among men and women in the United States. This kind of heart condition, recently mentioned, has a very direct relationship with the heart pathology studied in this work because coronary heart disease often leads to polymorphic VT and VF, which is the major cause of sudden cardiac death. "The estimated incidence of sudden cardiac death in the general population is 1/1,000 people per year in Western Europe".**1** (J. Fernández-Armenta et al., 2013)

It is important to define and describe the heart disease whose study has motivated this work; ischemic VT. Tachycardia is the medical term used when a patient presents a heart rate of more than 100 beats per minute due to effects unrelated to normal physiological stress. In this specific case of tachycardia, we are talking about a wide QRS tachycardia, which means that the QRS complexes of the cardiac signal show a duration of at least 120 milliseconds. Moreover, since it is a ventricular tachycardia, its focus of origin is on the ventricles, below the His bundle.

There are several types of VT. These can be classified according to their duration (sustained, arrhythmic, incessant) and according to the morphology of their QRS complexes (monomorphic, polymorphic, pleomorphic). The type of tachycardia suffered by each patient depends mainly on the physiological root that causes it. This study has focused on VT of ischemic origin, the most frequent variant, although it can also arise from dilated, hypertrophic or infiltrative structural cardiomyopathy, among others.

Cardiac ischemia, which commonly causes VT, appears in the ventricle due to coronary artery disease. Coronary artery disease consists of hardening and narrowing of the arteries of the heart, due to the accumulation of cholesterol and other materials, called plaque, in the inner layer of the

artery walls. This causes a partial or total obstruction that usually leads to ventricular ischemia. Ventricular ischemia occurs because blood flow to the heart is reduced, which impedes the cardiac muscle from receiving sufficient oxygen and the tissue suffers hypoxia, causing cell death in the affected tissue area and resulting in scarring.**2** *(Barrabés et al., 2011)*

The kind of ischemia I have described usually results in polymorphic VT, which is described morphologically by the constant variation of its QRS complexes in the cardiac signal, and VT, which causes the heart to beat with fast and erratic electrical impulses. As mentioned, polymorphic VT creates tachycardias in which the QRS complexes continuously change their morphology. It generates rapid and poorly tolerated arrhythmias and can also present different patterns of duration because it has an irregular rate. **1** *(J. Fernández-Armenta et al., 2013)*

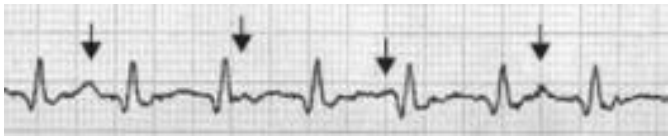

Figure 1: Diagram of an example of a wide QRS. Extracted from [3].

The pathophysiological mechanisms underlying this type of VT associated with coronary artery disease are complex. The whole mechanism is based on an abnormal automatism that arises at the edge of the ischemic tissue and causes focal activation. This automatism is explained by the fact that ischemia that affects myocardial tissue activates ATP-sensitive potassium channels. This excess of extracellular potassium in the cardiac muscle, together with the acidosis and hypoxia generated by the ischemia, causes depolarization of the myocardial resting membrane potential, which increases tissue excitability. Briefly, these conditions have the following effects on the affected tissue region: shortening the action potential, decreasing impulse conduction and prolonging the refractory period as a consequence of repolarization.**3** *(Benito & Josephson, 2012)*

After a coronary ischemic event, healthy tissue can be replaced by scar and border zone. Impulses can go throw these border zone areas slower and a slow conduction channel can be created. The re-entrant circuit generated based on this CC is the principal mechanism of ventricular tachycardia in chronic ischemic cardiac disease.

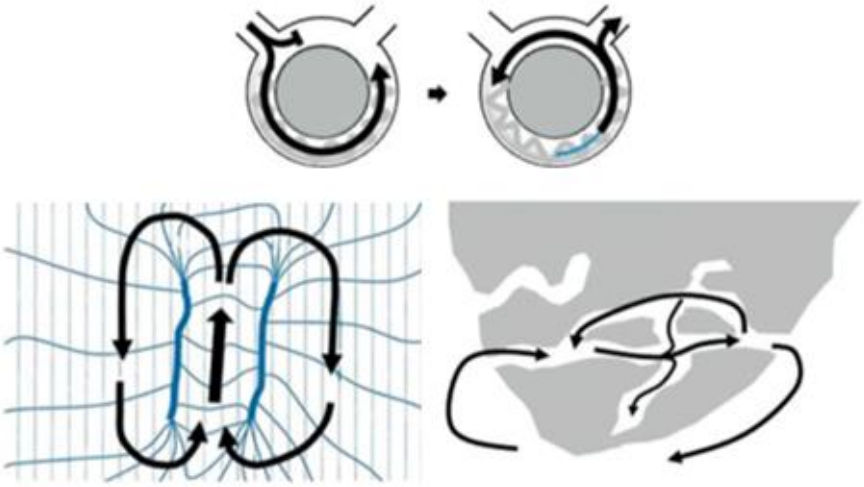

Figure 2: Schematic of three types of re-entrant circuits. Extracted from [3].

Re-entry is the most frequently observed arrhythmic mechanism in clinical arrhythmias and occurs when an isolated group of fibres that have not depolarized during the initial wave of depolarization are excited before the impulse is extinguished, since they still have time to depolarize. In this way, they can depolarize, prematurely, previously depolarized areas that have recovered from the initial depolarization.

For re-entry to occur, myocardial tissue with different electrophysiological, conduction and refractoriness characteristics is required. There must also be a zone of unexcitable tissue (due to anatomical or functional causes) that acts as a unidirectional conduction block around which slow conduction will circulate, allowing recovery of the proximal refractory tissue. **29***(Gaztañaga et al., 2012)*

According to a 2011 article by *A. Berruezo*, arrhythmogenic channels are defined as the orthodromic pathway (shortest route between two points) between abnormally activated regions near the scar. Two types of CC have been shown to be identifiable during sinus rhythm mapping: voltage-gated channels and late potential channels.**4** *(Berruezo et al., 2012)* As indicated by a 2014 clinical assay, late potential channels have a greater tendency to form substrate.**5** *(Juan Fernández-Armenta et al., 2014)* The substrate that forms these CCs can be found in the epicardium and endocardium, although it is more commonly found in the epicardium, according to some studies.**4** *(Berruezo et al., 2012)*

The arrhythmogenic channels are of great relevance when performing the most common treatment for this type of heart disease, radiofrequency ablation, since the entrance or beginning of these CCs, which are usually found in the corner of the scar with an 80% probability of occurrence, are the target for ablation. It has been demonstrated that ablating the entrance of the CC, a technique known as “dechanneling technique”, reduces the degree of radiofrequency application needed to eliminate the substrate that causes VT, increases efficiency and reduces the requirements of the procedure.**4** *(Berruezo et al., 2012)*

Because of the critical role that CCs acquire during the procedure and in its preparation, an optimal criterion should be followed to identify these CCs. Channels can be detected by contrast-enhanced MRI. Subsequently, a 3D reconstruction of the image can be made, a very useful resource that serves as a support for ablation guidance maps.**1** *(J. Fernández-Armenta et al., 2013)*

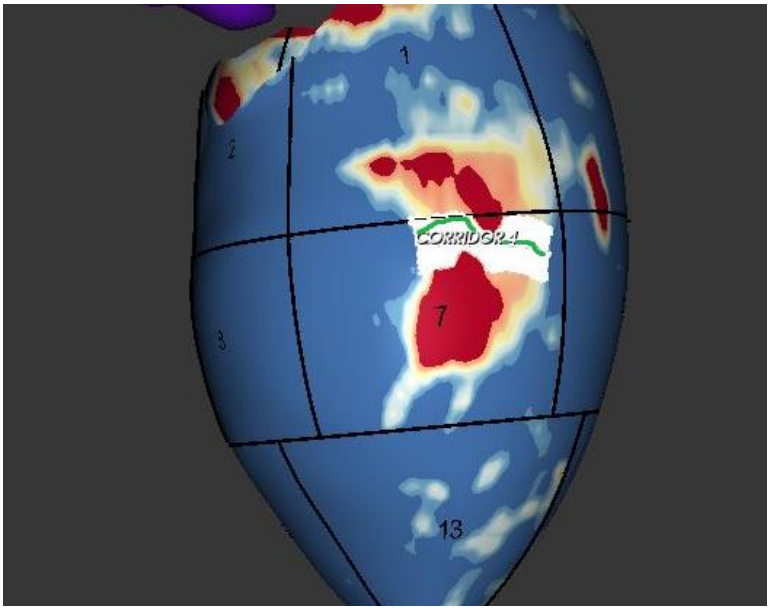

Figure 3: Model of a case of the study where an arrhythmogenic channel is highlighted in green.

2.1.2. Ventricular ablation

There are several treatment options for VT of ischemic origin. First, pharmacological therapy is usually given to the patient in an attempt to control the triggering cause and stop the acute ischemia. These treatments depend on the repolarization alterations shown by each patient. They may consist of magnesium supplementation or beta-blockers and amiodarone, which allow coronary revascularization.**1** *(J. Fernández-Armenta et al., 2013)*

If there is no improvement, the implantation and use of the famous implantable cardioverter defibrillators (ICDs) can be performed. These devices positively affect the survival of patients at high risk of sudden death. The main drawback of this method is that the user's quality of life may be adversely affected by the recurrent therapies required. Another negative aspect of these devices is that they generate a lot of noise in the 3D MRI images.**6** *(Acosta et al., 2016)*

In contrast, the most effective treatment for VT, which has developed exponentially in recent years, is ventricular ablation. Ventricular ablation consists of creating tiny scars over the ischemic myocardial tissue that represents the focus of the arrhythmia, specifically at the entrance to the CCs. This is done to block the abnormal signals that produce the quick, out-of-pace beats of the VT. In the past, open heart surgery was required to perform the ablation. Today it is performed percutaneously. This is an effective and highly safe procedure that consists of ablating the myocardium from the endocardial or epicardial surface by means of a catheter directed to the focus through the circulatory system. There are two ways of performing cardiac ablation: by radiofrequency, which uses thermal energy, and by cryoablation, which uses very low temperatures. In most cases, electroanatomical mapping techniques are used to guide interventions to the focus of the arrhythmia, allowing us to reconstruct, thanks to electrophysiology catheters, the cardiac cavities in three dimensions. These maps are used in conjunction with MRI techniques, which provide anatomical support. **7** *(Guandalini et al., 2019)*

2.1.3. Cardiac magnetic resonance with late Gadolinium enhancement.

In the last 30 years, cardiovascular MRI with late gadolinium enhancement has become the most widely used imaging technique for the diagnosis of the large majority of ischemic heart diseases. In addition, it is also a fundamental pillar for treatment, since its images contribute, by providing anatomical structure, to the creation of activation and substrate maps that guide ablation interventions using EP navigation systems.**8** *(Healthcare et al., 2014)*

Cardiovascular MRI is a technology whose purpose is to obtain three-dimensional anatomical images of the internal and external structures of the heart. It does not use harmful radiation, is non-invasive and has a high degree of spatial and temporal resolution.

Its technology makes it possible to differentiate and identify various types of tissues by taking into account the magnetic properties of the protons found in the water that compose the different tissues. The MRI equipment uses large magnets that create a high-powered magnetic field to ensure that the protons are aligned with the z-direction field. A radiofrequency pulse is then emitted through the patient, which generates another magnetic field perpendicular to the existing field, in the xy-direction. Then, the magnetic moment of the protons is altered and its direction varies in search of equilibrium.**9** *(Valbuena-lo, 2016)*

There are different techniques when emitting radiofrequency pulse sequences: spin echo, gradient echo or inversion recovery, among others. In the case of cardiovascular imaging, the inversion recovery pulse sequence is mostly used. This sequence consists of emitting a 180º inversion pulse that directs the protons in the opposite direction to the one they were in, before applying a spin echo sequence. The spin echo then emits a 90º pulse and a 180º pulse before receiving the signal (echo) that will provide information on the magnetization of the protons. The time between the first inversion pulse and the application of the spin echo sequence is called inversion time (IT). The advantage of this sequence is that when the spin echo is emitted, after a certain inversion time, the z-component of the proton magnetization of the water composing the different tissues is already differentiated, due to the difference in the intrinsic T1 relaxation time of each tissue. This factor leads to an improvement in image contrast, which can be adjusted by modifying the inversion time.**10** *(Young, 1999)*

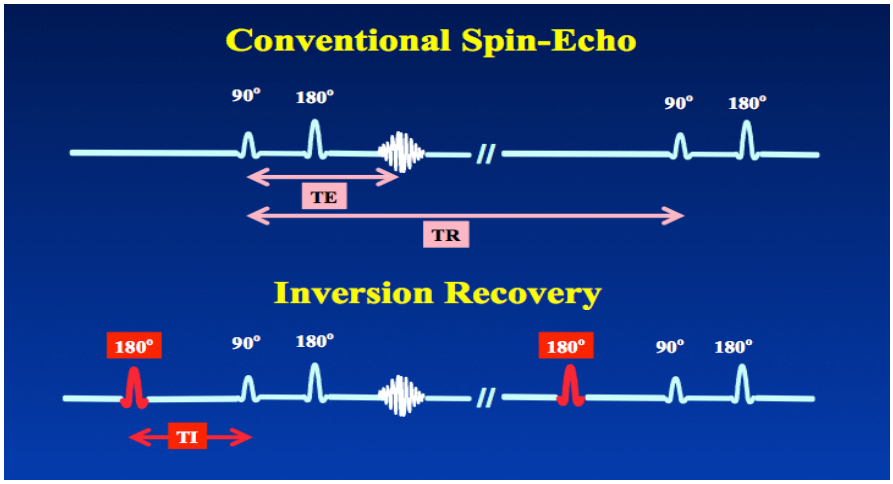

Figure 4: Comparative diagram of spin echo (top) vs. inversion recovery (bottom). Obtained from [10].

When the pulse is no longer emitted, a radiofrequency sensor, containing an electromagnetic inductor, is able to detect the energy released by the protons as they realign again with the magnetic field. The chemical nature of the molecules that make up each type of tissue determines the relaxation time T1 (time it takes for the z component of the proton magnetic moment to acquire 86% of the maximum magnitude it had before the pulse), the relaxation time T2 (time it takes for the xy component of the proton magnetic moment to acquire 37% of the magnitude it had initially after the pulse) and the amount of energy released during the realignment process. **9** *(Valbuena-lo, 2016)*

This technology uses voxels as the volumetric unit of measurement, which are the cubic units that conform the anatomical slice that is being captured. Therefore, the MRI obtains the magnetization values (z component of the magnetic moment if it is a T1-weighted type MRI and xy component of the magnetic moment if it is a T2-weighted type MRI) of each of the voxels. To determine the spatial location of these voxels and the slice thickness, gradient coils are used to generate a gradient of the applied magnetic field in z or xy direction, so that the value of the received signal depends on the topography of the voxel.**9** *(Valbuena-lo, 2016)*

Finally, a reconstruction technique is able to obtain tissue's protons magnetization measurements and their position from the above-mentioned data to translate them into pixel intensity and create the image.

To obtain a quality, non-blurred image, it is necessary to ensure that the patient remains immobile during the examination. In addition, the introduction of GBCA 25 years ago ushered in a new era of diagnostic capabilities for MRI. Late gadolinium enhancement, which involves administering the GBCA intravenously before or during the examination (usually observed 10 to 20 minutes after administration), dramatically accelerates the rate at which protons realign with the magnetic field, thus shortening the T1 relaxation time of the water containing tissue that has bound to the gadolinium molecule. This has the effect that the magnetization captured in the areas close to the gadolinium has a higher value and, consequently, that area is brighter.**11** *(Chou et al., 2013)*

The purpose of late gadolinium enhancement is to directly visualize the pathophysiological substrate that gives rise to the heart disease, meaning the scar caused by myocardial fibrosis. This is because gadolinium has an affinity for fibrotic-necrotic tissue and highlights its spatial and temporal distribution, generating a contrast with respect to healthy tissue, with which it has no affinity and, therefore, appears darker. To achieve optimal contrast in the image, it is necessary to determine an adequate inversion time so that the vertical magnetization values of the different tissues are sufficiently differentiated from each other, to determine the optimal moment to administer gadolinium and to perform a correct reconstruction, apart from image processing.**8** *(Healthcare et al., 2014)*

2.1.4. Reconstruction methods

Reconstruction plays a fundamental role in the clinical use of MRI. This process performs the function of converting the data obtained during the test (raw data) into an image for clinical interpretation. This process consists of a program implanted in the MRI diagnostic device that involves multiple signal processing steps and has a considerable impact on image quality.**12** *(Hansen & Kellman, 2015)*

There are several methods of MRI reconstruction. The main objective is to compare the two inversion recovery resonance reconstruction methods, MAG and PSIR.

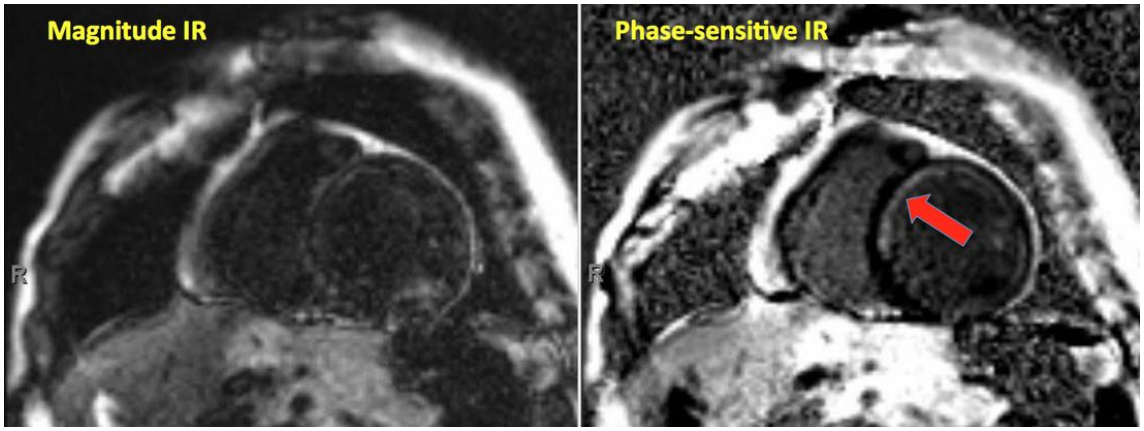

Figure 5: Magnitude and PSIR image comparison. Left: Magnitude. Right: PSIR. The red arrow indicates the position of the fibrotic zone. Obtained from [15].

2.1.4.1. Magnitude reconstruction sequence

Usually, MRI using inversion recovery sequences employs Magnitude reconstruction to translate the signal captured during the scan into pixel intensity. In this method, the brightness of the pixels depends only on the magnitude of the vertical magnetization (or longitudinal magnetization) of a tissue, not on its polarity. In other words, two tissues whose magnetization at inversion time point in equal but opposite directions along the z-axis will be depicted in the same shade of grey and will therefore be indistinguishable.**13** *(Juan et al., 2015)*

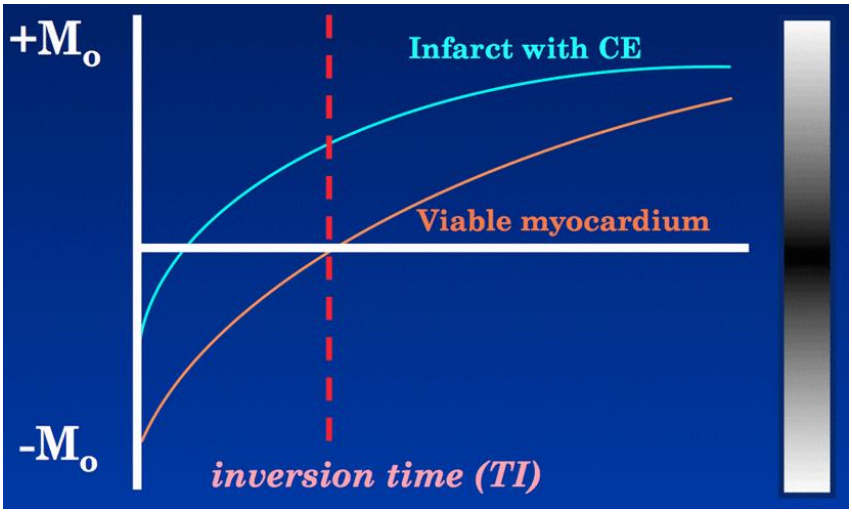

Figure 6: Explanation diagram of the Magnitude reconstruction system. Y-axis = longitudinal magnetization. X-axis = inversion time. Obtained from [18].

It is interesting that healthy tissue has a low intensity value, to make it look dark and improve interpretation. This is achieved by determining an appropriate inversion time. Although the optimal inversion time for viable myocardium to have zero longitudinal magnetization magnitude depends on contrast dose and body weight, it can be determined with an inversion time mapping sequence, based on the principle developed by Lock and Locker in the 1970s.

Today, the technique is called TI scout by *Siemens* or Cine IR by *GE*. The technique consists of an ordered and segmented series of echo images, of cine GRE or b-SSFP type, obtained over various heartbeats. Each of these echo images corresponds to a different inversion time value. Finally, an algorithm evaluates this series to determine the optimal inversion time.**14** *(Vogel-claussen et al., 2006)*

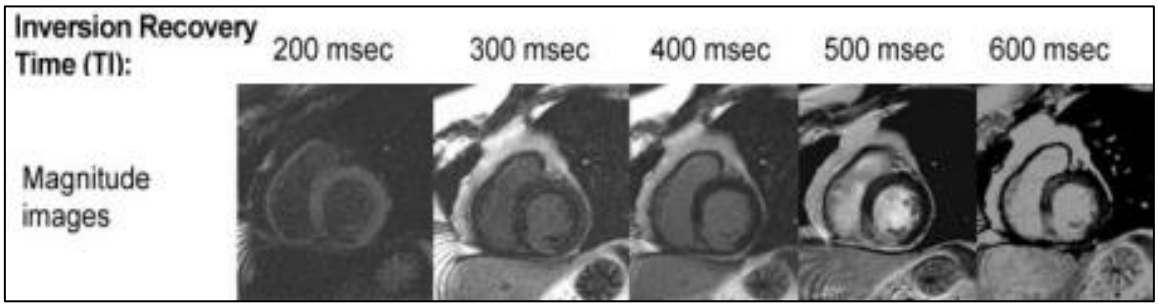

Figure 7: Series of the TI-scout technique in Magnitude sequence. Different inversion times in each shot. Extracted from [15].

2.1.4.2. Phase sensitive IR (PSIR) reconstruction sequence

The phase sensitive IR (PSIR) reconstruction method preserves the positive and negative polarities of the z-component of tissue magnetization as they recover from the initial 180° reversal pulse. With this technique, tissues with more negative longitudinal magnetizations always appear darker than those with more positive magnetizations. Therefore, fibrotic tissue always has a higher and brighter signal, as it binds to gadolinium that accelerates its magnetic recovery, promoting the positive polarity of the tissue.

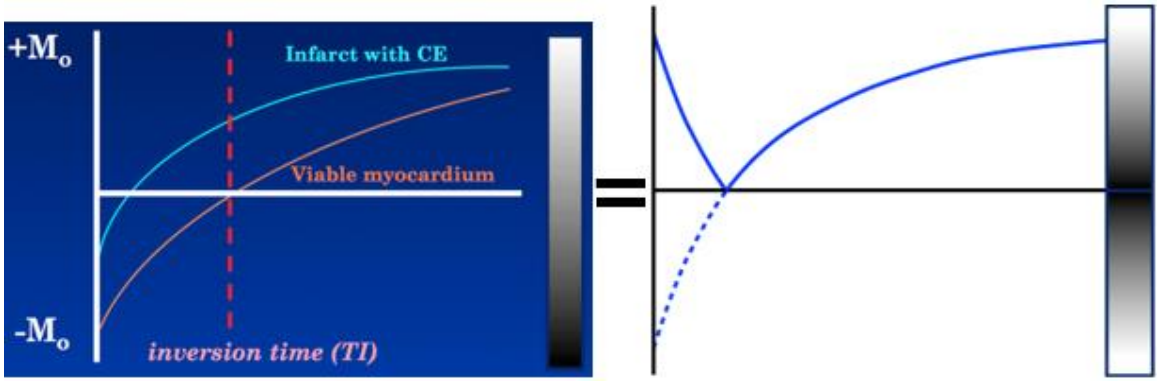

Figure 8: Explanation diagram of the PSIR reconstruction system. Y-axis = longitudinal magnetization. X-axis = inversion time. Left: longitudinal magnetization in relative value. Right: longitudinal magnetization in absolute value Obtained from [18].

In contrast to MAG reconstruction, the PSIR technique gives good results over a relatively wide range of inversion times.**15** *(Huber et al., 2005)*

Although PSIR reconstruction makes it possible to produce excellent quality contrast-enhanced images without using an inversion time mapping sequence, PSIR images will be even better if an optimal inversion time estimation is first performed.

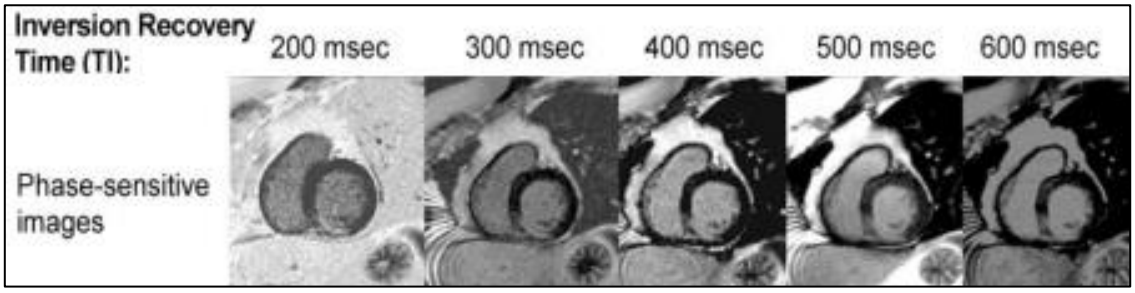

Figure 9: Series of the TI-scout technique in PSIR sequence. Different inversion times in each shot. Extracted from [15].

2.1.5. Representation, segmentation and interpretation techniques

Once the patient undergoes a 2D cardiac MRI examination with late gadolinium enhancement, a collection of bidimensional images is acquired, created using a specific reconstruction method. Each of these images captures the same plane (specific to the area under study) at different positions with respect to a specific axis. Normally, the distance between each of the layers is approximately 2 to 3 millimetres. The format of these images is usually a DICOM file.

Next, it is required a software that is capable of translating these radiological images into a comprehensible representation of the ventricular substrate, so that its structure can be visualized and the properties of each region can be correctly interpreted. In addition, it is essential to segment the section of clinical interest and to conveniently adjust the parameters that affect the correct visualization of the myocardial scar.

Therefore, the purpose of this step is to represent the images in such a way that the anatomy of the LV is perfectly understood, the topology of the substrate (healthy regions and scars) can be identified with extreme precision, and the detection of CCs is possible. On the one hand, this process is necessary for clinicians to perform a pre-intervention study and choose the best approach for the operation. On the other hand, it also serves to create a structural support for the electroanatomical guidance maps required during the intervention. And, on the other hand, to repeat the representation with a new acquisition after the intervention and to be able to estimate the post-intervention change or improvement.

The literature on MRI image segmentation can be divided into two categories: single-image or grayscale segmentation, where a single 2D or 3D image is used, and multispectral image segmentation, where multiple images with different grayscale contrasts are used. Each category can perform segmentation using different methods and can combine manual segmentation techniques with automatic segmentation techniques performed by software. Automatic segmentation programs work by extracting and selecting features, which will provide the measurement vectors on which the process will be based. These features can be, for example, the intensity of the pixels and, with them, other features such as edges and textures can be calculated. Then, a function groups the pixels into sections, depending on the selected features, and defines the boundaries. Finally, tissue classification and identification is performed using defined algorithms, which can be based on threshold detection, boundary detection, edge detection, pattern recognition or algebraic approaches.**16** *(Hal & Jr, 1995)*

2.1.5.1. ADAS 3D

In this project we will work with the 3D segmentation and representation software ADAS-3D to perform this function. ADAS-3D is a program that allows the visualization and determination of the structure of the fibrotic substrate of the LV from MRI images in DICOM file. This software works with a segmentation method that combines a manual part, in which the user must set landmarks and delimit the target sections layer by layer, with an analytical detection technology that operates by means of algorithms in a topological space. This technology is capable of making a three-dimensional construction of the segmented region and recognizing the nature of the substrate through an analytical program that studies the brightness intensity of each pixel, averages it and allows thresholds to be set to discriminate between healthy tissue, fibrotic tissue and BZ. In addition, it has the great advantage of being able to detect arrhythmogenic channels by analysing the 3D structure of the tissue. **17** (*ADAS 3D LV: Technology*, n.d.)

2.2. State of the situation

Regarding the current situation of the two methods of cardiac MRI reconstruction described in the previous section, it can be affirmed that they constitute an essential tool for clinical trials of heart disease and that both are used on a daily basis.

In recent years, a large number of comparative and evaluative studies have been carried out on these sequences. The vast majority of these investigations, in summary, consist of performing MRI scans on a group of patients who have suffered a cardiac structural pathology and applying the two reconstruction methods and then measuring certain parameters (Contrast-to-Noise ratio, for example) that serve as a reference for a subsequent statistical study (t-student) to evaluate the efficiency and quality of each method.**15** *(Huber et al., 2005)*

The general conclusions regarding the comparison of the two methods determine that the advantages of PSIR lie in four main factors: it generates a more consistent image quality showing more sensitivity to contrast changes, decreased background noise, drastically reduces the apparent size variation of the infarcted tissue, and dispenses with the need to choose the optimal inversion time required by the MAG technique. The last of these advantages means that the patient does not have to undergo as many scans and it speeds up the diagnostic process considerably.**18** *(Kellman et al., n.d.)*

Even so, PSIR has not yet fully replaced the MAG sequence for other reasons. It turns out that the PSIR technique is somewhat difficult to implement because the sequence suffers from errors due to phase artifacts and requires long analysis times. Sources of phase errors include patient-related variations, coil loading and sensitivity, the echo not being centred in the readout window, and hardware-induced phase shifts. In all cases a phase correction algorithm must be employed, which may involve the acquisition of an additional reference image, or an estimation of the phase map.**19** *(Moran et al., 1986)*

As an aside, MAG reconstruction does not require such a sophisticated post-processing technique. In addition, MAG reconstruction allows adjustment of TI for selective nulling of tissues such as fat or blood, which can be useful at certain locations on the substrate where there is little contrast. Selective nulling techniques are not possible with PSIR.**19** *(Moran et al., 1986)*

Therefore, validate if the PSIR technique is as useful as MAG for channel detection may be more useful for which structures and locations to study may be of great advantage to all healthcare sectors using cardiac MRI. Specifically, the aim of this project is to find out which of the two methods is more effective in determining the CCs in ischemic VT, a study which, above all, will be of benefit for guiding the intervention, the ablation.

3. ANALYSIS OF THE MARKET

The study and discussion of the different reconstruction techniques currently on the scene has become a very busy field of research. This concern emerged due to the impact caused by the introduction of the PSIR technique in the market in year 2000. This was a revolution due to all the advantages that it seemed to present with respect to the Magnitude reconstruction technique, which was the one that was strongly established in the sector.

The interest in investigating each technique and seeing which is more useful in specific cases is due to the importance of reconstruction in the diagnosis and intervention of heart disease. In addition, it is also an advantage over catheterization maps because it is a non-invasive technique.

Most of the sectors targeted by advances in this field of research are medical centers or hospitals, image processing software, MRI technology companies or medical imaging clinics.

3.1. Historical evolution and future prospects of the market

It has been 40 years since the writing of this paper that Dr. Raymond Damadian demonstrated that MRI could be used to detect disease, because different types of tissues emit different signals in response to an applied external magnetic field. Since then, MRI has become one of the most efficient and advantageous techniques for acquiring anatomical images, since it achieves images with a very high quality resolution and does not emit harmful radiation or cause negative effects for the patient. The large number of benefits that have been achieved with this diagnostic technique in the world of medicine has favoured its exponential development. This technology has established itself around the globe, has been manufactured and marketed by numerous companies (*eSAOTE*, *Canon*, *Philips*, *GE*) and has diversified by creating specialized devices to analyse different areas of the body and study a wide range of diseases.

More than 30 years ago, the GBCA was introduced to improve the quality of the image obtained and was a major advance in MRI, especially for the detection of heart disease. The first GBCA was dimeglumine gadopentetate (from Bayer Healthcare), which was approved in the United States in 1988. From this time, several other agents followed including: gadoteridol (from *ProHance*), gadodiamide (from *GE Healthcare*), gadovertamide (from *Mallinckrodt Pharmaceuticals*) and, more recently, gadoteride meglumine (from *Guerbet*). As all these agents have the same concentration, in 1990 the value of 0.1mmol/kg was assigned to standardize the amount of a single dose.**20** (*Gadolinium-Based Contrast Agents: What Does "Single-Dose" Mean Anymore?*, n.d.)

From the earliest models of MRI imaging equipment, the method used to reconstruct the image was based on the magnitude of the vertical magnetization of the tissues. It was not until 2000 that Jingfei Ma, PhD in imaging physics at the University of Texas, patented the first model for reconstructing MRI taking into account the polarity of the magnetization, beyond its magnitude.**21** (*Patent_PSIR*, 2000) Even so, Jignfei Ma did not publish his first paper about this new technique until 2005.**22** *(Ma, 2005)*

The great progress that this technology has undergone to date does not mean that there are no areas for improvement or that progress has stopped. In today's market there are many prospects for the future of these techniques. The aim is to perfect all processes. Specifically, looking at the reconstruction stage, the market is interested in having stipulated, by means of scientific demonstrations, which method is most useful in each situation, depending on the affected area, the patient's conditions, the specific pathological aspect in question. A future perspective is to define which of the techniques is most useful to determine a specific structure to be studied, such as CCs. It is also expected that the investigation of these issues will lead to a solution or improvement for the errors still present in both reconstruction techniques studied in this project, such as the noise created by phase artifacts in the PSIR, or to integrate an algorithm in the MAG that directly determines the optimal inversion time. On the other hand, it is also intended to determine a correct configuration for the images obtained through both segmentation techniques, including the optimal threshold adjustment. In no case, the aim is to substitute one technique for the other in order to standardize the processes nor to have a dominant technique, because, for example, although PSIR offers higher contrast quality, sometimes it is necessary to ensure the magnetization cancellation of a specific tissue and this is done with the MAG reconstruction, together with a study of the estimation of the appropriate inversion time.**23** *(Hou et al., n.d.)*

4. ENGINEERING OF CONCEPTION

4.1. Segmentation method

4.1.1. Study of solutions

In the process of acquiring diagnostic images, the processing and segmentation stages have a great relevance because they directly influence the final result. Therefore, it is important to choose correctly what approach these phases will have so that the final images only depend on the reconstruction sequence applied, which is the objective of the project. The goal of segmentation is to obtain a segmented image of the LV.

Nowadays, the segmentation process is carried out automatically, using specialized software, or semi-automatically, using proposed segmentation algorithms. In order to determine which path this part of the project should take; it is necessary to focus the study of solutions on the choice of the appropriate method that performs this function as accurately as possible. **24** *(Zhuang & Shen, 2016)*

The most widely used cardioresonance image segmentation programs on the market are the following:

- CardiacSegmentationPropagation. It consists of a segmentation method with spatial propagation that is applied from Python and is based on deep learning. It is free of charge.
- Segment CMR. It is a well-validated comprehensive software for cardiovascular image analysis. It is freely available for research purposes, provided that research publications related to the software are cited.
- ADAS-3D. This software represents radiological images to interpret the ventricular substrate. The myocardium of the ventricle is visualized by breaking it into easy-to-understand layers to reveal the structure of the scar. Collaboration with Hospital Clínic.
- Arterys CardioAI. It is a cardiac MRI software that drives workflow with deep learning and supercomputing in the cloud. It serves to analyse the heart and its major vessels using multi-slice, multi-phase, velocity-coded cardiovascular MRI. It provides clinically relevant and reproducible quantitative data and has been tested and validated on MRI images acquired from 1.5T and 3.0T MRI scanners.

4.1.2. Proposed solution

The proposed solution in terms of the choice of segmentation software was **ADAS-3D**. The main reason for this decision is that ADAS-3D is the platform used by the arrhythmia unit of the Hospital Clínic, so they can offer basic training in its use.

It also has numerous advantages over the other options, for example, it constructs a three-dimensional representation of the segmented area in which the amount of gadolinium-bound myocardial tissue (fibrotic tissue) can be visualized from different perspective angles over the

entire surface of the LV and at different levels of thickness. It features an interactive interface with animations that shows in a very clear and compressible way the topology of the ventricular tissue.

In addition, it is the only program that allows direct detection and determination of CCs at the edge of the fibrotic tissue. The software is able to visualize them selectively in three dimensions and make a quantitative examination of them to know their mass as well as other characteristics. This fact is a very positive factor for me in this study.

Figure 10: ADAS-3D logo. Extracted from: https://www.adas3d.com/en/adas-vt-product.html

4.2. Validation reference

4.2.1. Study of solutions

The fundamental element of this solution study is to clarify which reference will be used to validate the feasibility of the PSIR reconstruction sequence. What is needed is a reference whose technology is well established, has been in use for years without problems, and is validated, certified and referenced. Mainly, the techniques that are used in this particular field of application and that meet the requirements and properties mentioned above are the already explained Magnitude reconstruction sequence and the three-dimensional electroanatomical maps created by catheterization.

Electroanatomical mapping systems have represented the great step forward in cardiac ablation technology. They allow real-time localization of catheters in space by triangulation. They perform a three-dimensional reconstruction of the cardiac anatomy, thanks to the use of diagnostic catheters. In addition, the electrical information of the heart can be measured and projected onto the anatomical map, thus obtaining an electroanatomical map. They allow the map to be merged with preoperative MRI or CT scans, which provide the necessary structural support. Navigators can operate according to different principles:

- *Magnetic localization.* It is formed by a plate, containing 3 electromagnetic field focuses, which is placed under the patient's back. The catheter, which must have a magnetic sensor, has built-in magnetic coils in which currents will be induced depending on the relative position between the electromagnetic sources and the tip of the catheter. This position is inferred by triangulation.
- *Localization based on currents or impedances*. The patient has 6 patches attached to his back, which function as receivers of high-frequency signals emitted by the electrode of each catheter.
- Current navigators use *both principles* of catheter visualization.

The types of three-dimensional anatomical maps that we can obtain of the myocardium by navigation are these:

- *Anatomical*. The interior of the heart is scanned with the diagnostic catheter. Only the position of the catheter is taken into consideration and, from it, the map of the cardiac anatomy is reconstructed. An anatomical ablation will be, for example, atrial fibrillation, since we need to locate the pulmonary veins and burn around them, therefore, we do not need electroanatomical maps because we do not need to locate a focus of automatism.
- *Voltage or substrate*. They can be bipolar or unipolar. Based on the maximum voltage of the signal at each point.
- *Activation*. The time elapsed between a fixed reference and the electromyogram arriving at the mapping catheter is measured. **25** *(Vanegas et al., 2016)*

This solution study should determine which of the two proposed techniques, MAG MRI reconstruction sequence or electroanatomical mapping by catheterization, will be more suitable for validating the PSIR sequence in determining the arrhythmogenic channels.

4.2.2. Proposed solution

After a deliberate study of the situation and evaluating numerous aspects of each option, it was decided that the maps created from images constructed with **Magnitude sequence** will be the validation reference for this study on the PSIR sequence.

The main reason for this decision is the fact that the MAG sequence also works with cardioresonance images, while the electroanatomical maps do not. This implies a level of similarity, in terms of the expected results, that will provide rigor to the study and reduce its perplexity. Another factor that has made this decision an advantage for the work is the fact that there is so much documentation that references and certifies the quality and safety of its operation, since it has been used for years in both the clinical and research fields.

On the other hand, although the electroanatomical maps allow high-quality visualization, their acquisition entails an excessively high level of difficulty and additional time for the framework of this work.

5. DETAILED ENGINEERING

This section is key for the understanding of how the project was carried on. Here, I will explain in detail the materials and methods I have followed to study the images of patients' LVs taken with both methods. The information of this section is divided in materials, methods, results and discussion.

5.1. Materials

The materials used for the development of the project have been:

- 60 full MRI ventricular acquisitions of 30 real patients.1 sample sequenced with MAG and 1 sample sequenced with PSIR, for each patient.
- ALMA software. The network used by the Hospital Clínic as a database to store and retrieve patient information.
- The ADAS-3D software. The graphic support that allows segmentation and representation in three dimensions of myocardial images taken by diagnostic imaging techniques, MRI.
- SPSS software. A program that allowed me to save all the data and perform the subsequent analytical study.
- RStudio. RStudio is an integrated development environment for the R programming language, dedicated to statistical computing and graphics.

5.2. Methods

5.2.1. Overview

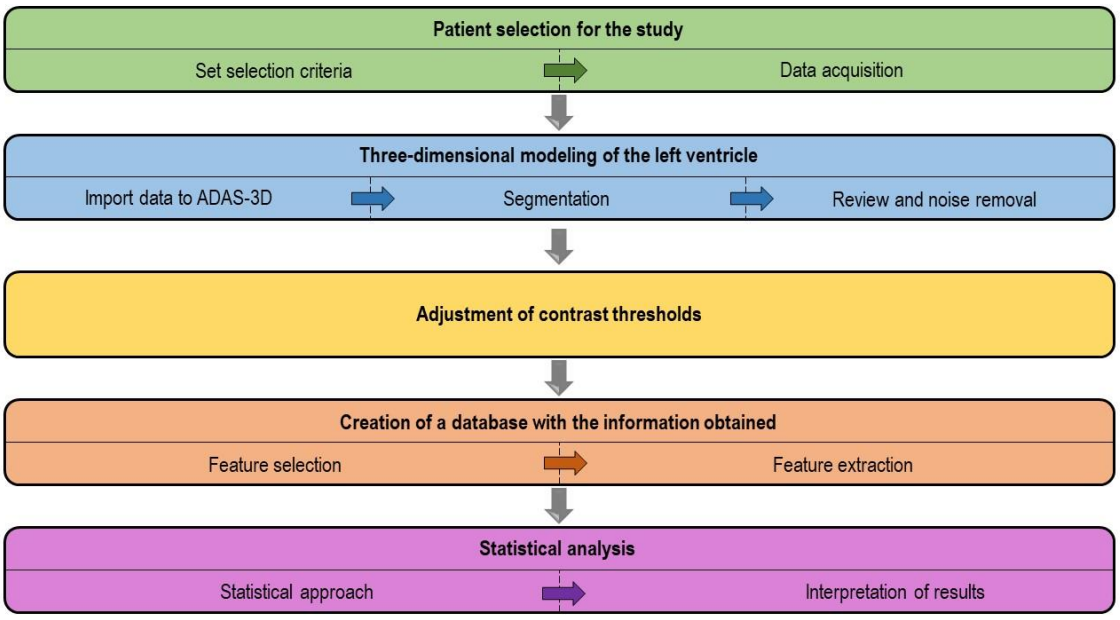

Figure 11: Flowchart of the methods followed in the experimental part of the project.

5.2.2. Patient selection

The first step was to select the patients who provided the ventricular images needed to develop the experimental part of the project.

5.2.2.1. Selection criteria

Initially, I have had to determine the number of samples to be treated, taking into account two aspects: the size of the sample is directly proportional to the precision of the results and the time dedicated to the work, as well as the number of patients, is limited. After assessing the situation, we have decided to choose a sample size of 30 patients, leaving a margin in case some of them were not valid for the study due to problems that might occur. At the end of the work, we have been left with 21 patients valid for the study, a sample size that seems to us to be quite acceptable.

The next step has been to determine which characteristics the patients in consideration had to meet. The selection criteria followed were as follows:

- Patients with ischemic VT.
- Patients with images obtained by 2D MRI reconstructed using the MAG sequence and PSIR.
- Patients with pre-intervention images.
- If possible, patients with MAG images already segmented, in order to work in advance.

We have not taken into account criteria of sex, age or ethnicity because they do not constitute a conditioning variable for the study.

Finally, we selected patients who had already undergone surgery for ischemic ventricular tachycardia by ablation in the arrhythmia unit and who, therefore, already had the MRI sequence with MAG segmented and analysed.

Once the patients on which the work was based had been selected, I had to create a database in SPSS with the list of patients, their identification number and the images taken. The purpose of this list was to facilitate the follow-up of the development of the work for each case.

5.2.2.2. Data collection

Next, I have proceeded to download the image compilations of each patient, which are in DICOM file. These data are stored in the ALMA support. Once the ALMA program was opened, I have had to look for the patients preferably by their identification number in the "*Consulta - Descarga*" section, having the *MR* modality marked.

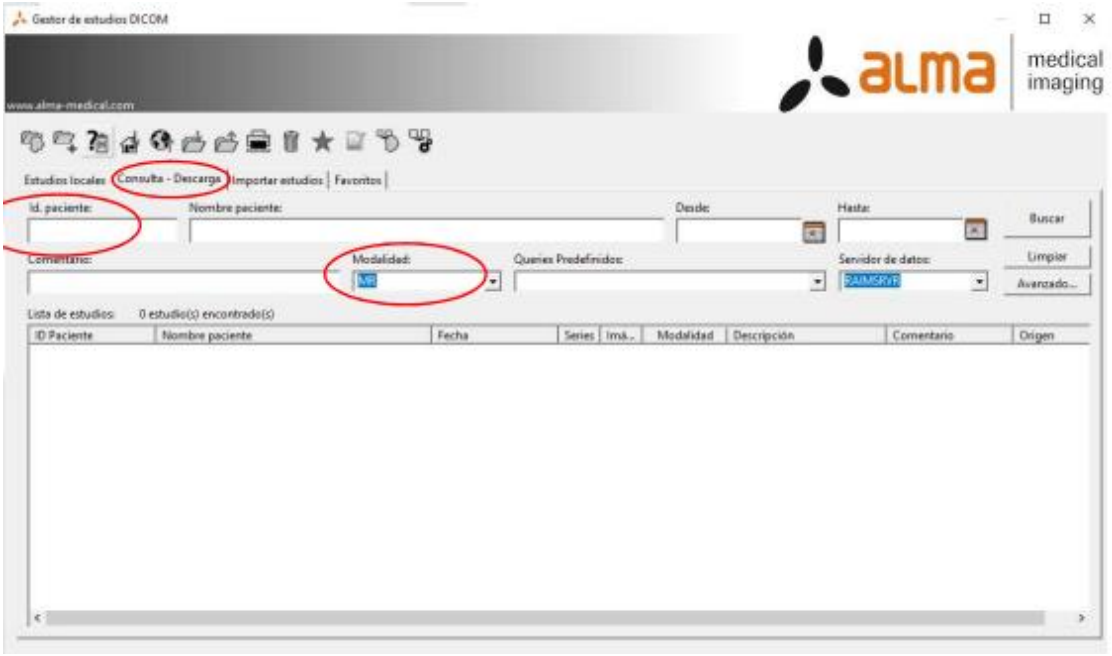

Figure 12: First step of Data Collection in ALMA support.

Then, the next step has been to look at the date of acquisition of the images to access their content and once inside download the DICOM files corresponding to the images obtained by MAG or PSIR, separately. There are usually 15 to 20 DICOM files for each acquisition with each reconstruction method.

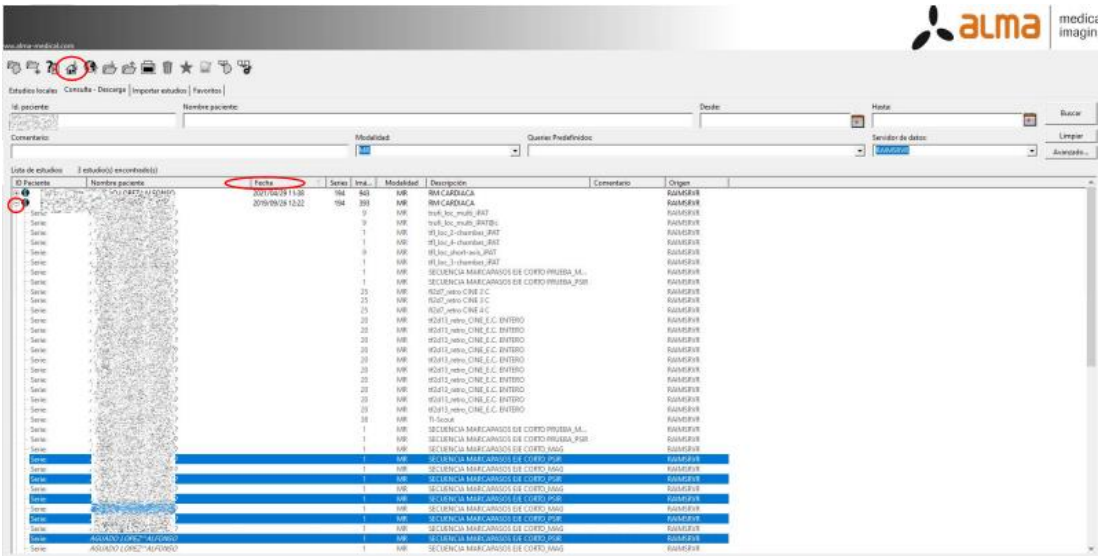

Figure 13: Second step of Data Collection in ALMA support.

Once the DICOMs had been downloaded to ALMA, the last step has been to export all the information to a repository folder where to save the data organized by patient and reconstruction method. In addition, I have had to take care to deactivate all anonymization options.

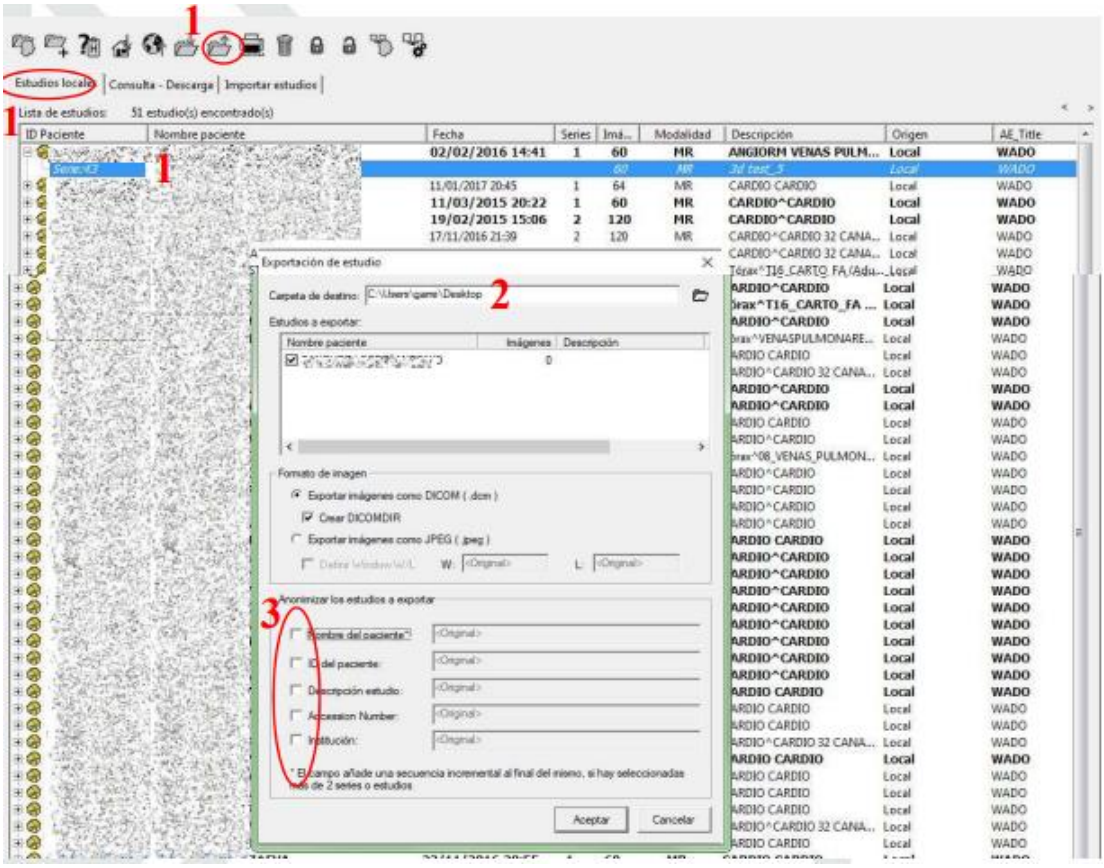

Figure 14: Third step of Data Collection in ALMA support.

5.2.3. Construction of the three-dimensional model of the LV

To translate the two-dimensional images from the DICOMs into segmented representations of the LV to study its composition and to obtain data to help me compare the two sequences, I have used the 3D segmentation and rendering program specialized in myocardial structures ADAS-3D. It is an imaging platform intended to help healthcare professionals visualize fibrosis, wall thickness, and myocardial and surrounding anatomical structures.

5.2.3.1. Import data to ADAS-3D

The first step was to import the DICOM files into the program, selecting the folder where they are located and indicating beforehand that they are two-dimensional MRI.

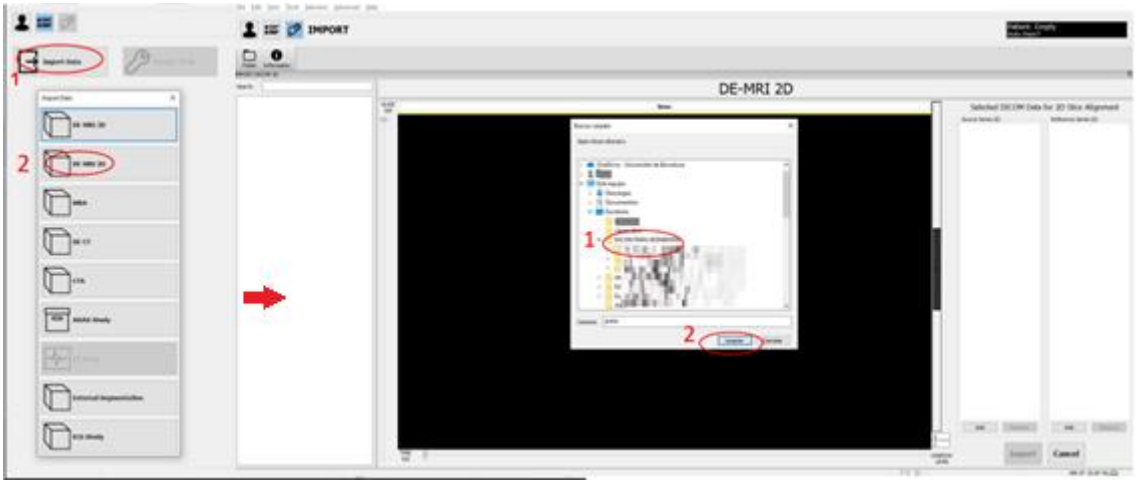

Figure 15: First step of importing data to ADAS-3D program.

Then I have had to add the imported images in ascending layer order. To do this, I have used a program function called *sliceposition* that tells me in which position of the axis each image is located. The reference I have followed to order the layers has been the fact that the distance between them is usually from 2 to 4 millimetres approximately, therefore, knowing that and the position of the images on the axis I have been able to order them correctly.

The main problems I have encountered have been collections of disordered images and repeated layers, in which I have had to choose by eye the one with the best quality.

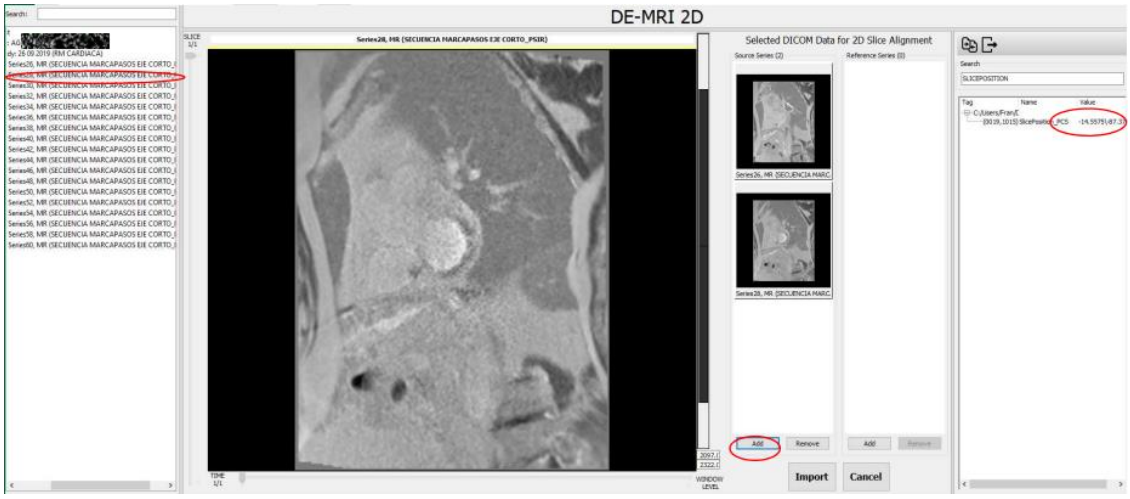

Figure 16: Second step of importing data to ADAS-3D program.

Then I have had to click *Import* and save the study in an organized repository folder and always with the same name, "*TV_PRE_PSIR*".

5.2.3.2. Segmentation

Once the study is created, we have to start a new analysis of the LV. Thus, we will step to the beginning of the ventricle segmentation process.

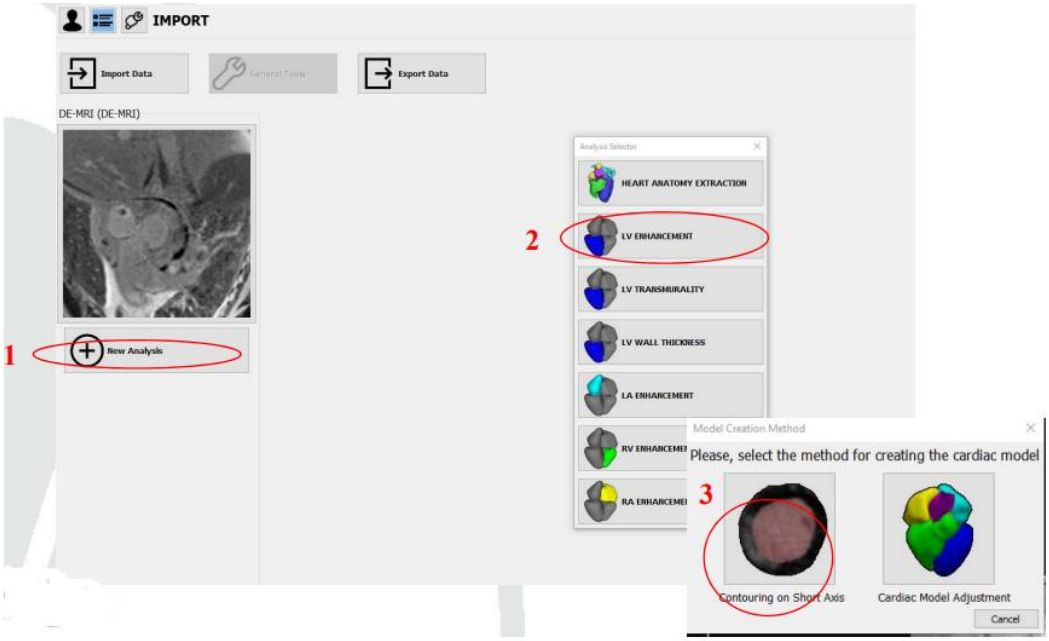

Figure 17: First step of segmentation in ADAS-3D program.

1. Set landmarks

The first step is to set the landmarks. The landmarks are points of the anatomy of the LV whose location in the layers provides the program with a first approximation of the morphology of the structure.

The landmarks to be placed in the layers are the following:

- The beginning of the Aorta (found in the upper layers).
- The mitral (found in the upper layers).
- The apex of the LV (found in the lower layers).
- The tricuspid (found in the upper layers).

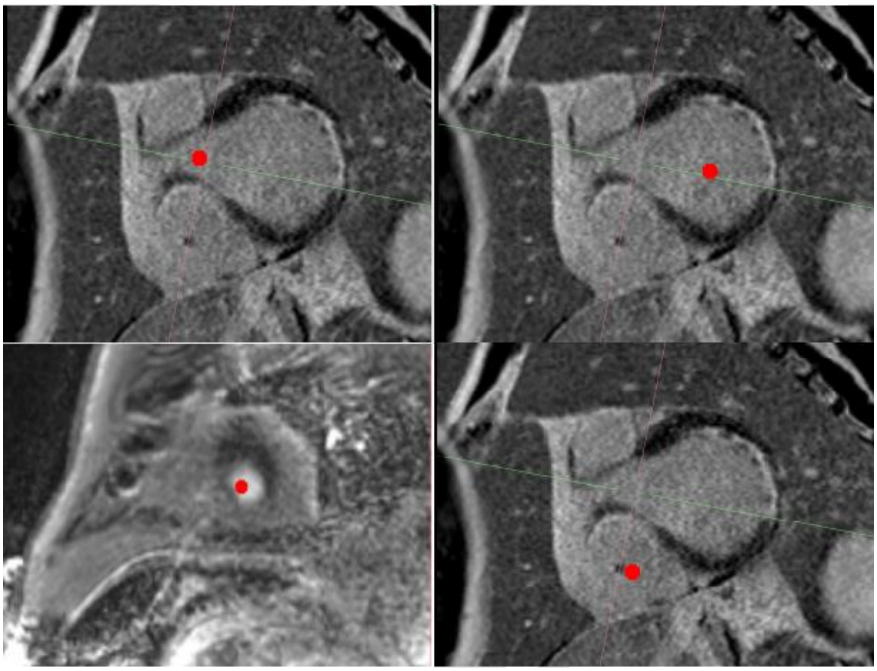

Figure 18: Location of the landmarks. Up-Left: Aorta. Up-Right: Mitral. Down-Left: Apex. Down-Right: Tricuspid.

2. Delineate contours of the endocardium and epicardium

The next step consists of delineating the contours of the ventricular endocardium and epicardium layer by layer. The delineation process is performed by drawing the outline with the cursor in each of the layers, starting with the apex and ending with the emergence of the Aorta. This technique is highly dependent on experience and practice. It is important to know well the anatomical structures, the pixel intensity that corresponds to each type of tissue, to know how to differentiate fibrotic tissue from healthy tissue and to recognize how the different types of artifacts that distort the image are manifested.

It is important to keep in mind that the layers must be aligned after defining the outline of the endocardium and epicardium so that the representation of the LV is well formed , with the layers correctly overlapping.

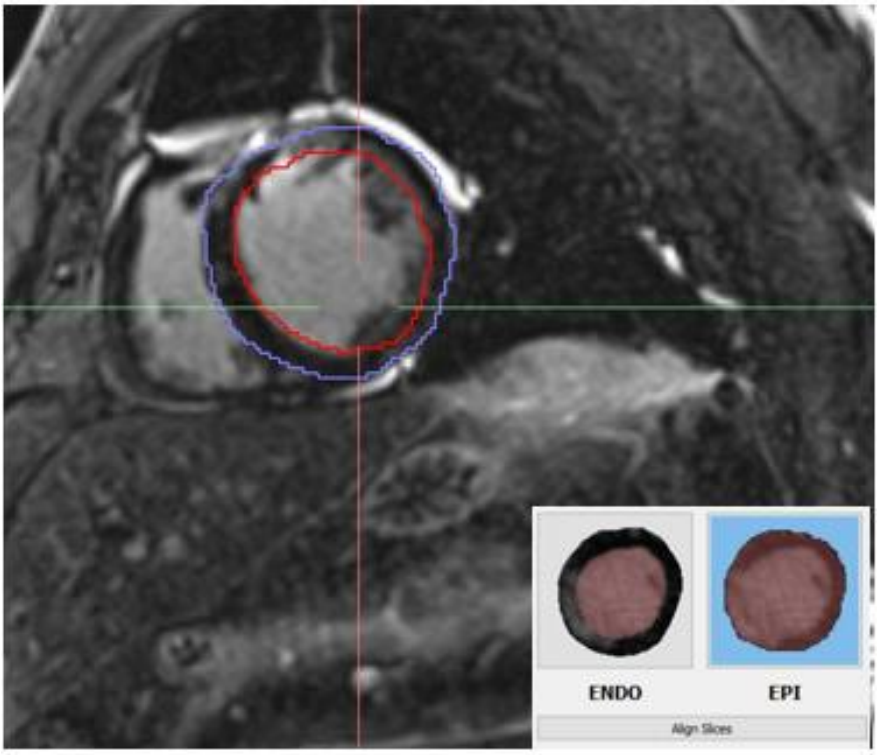

Figure 19: Process of delineating the contours during the segmentation stage in ADAS-3D.

3. Model adjustment

The last step of the segmentation is the adjustment of the model. The objective of this part is to deform the previously defined contour to make it more similar to the one observed in the images of each layer. This results in a more realistic model and a more accurate representation.

To do this, I have modified the traced perimeter of the endocardium and pericardium layer by layer to better match the actual shape of the patient's LV.

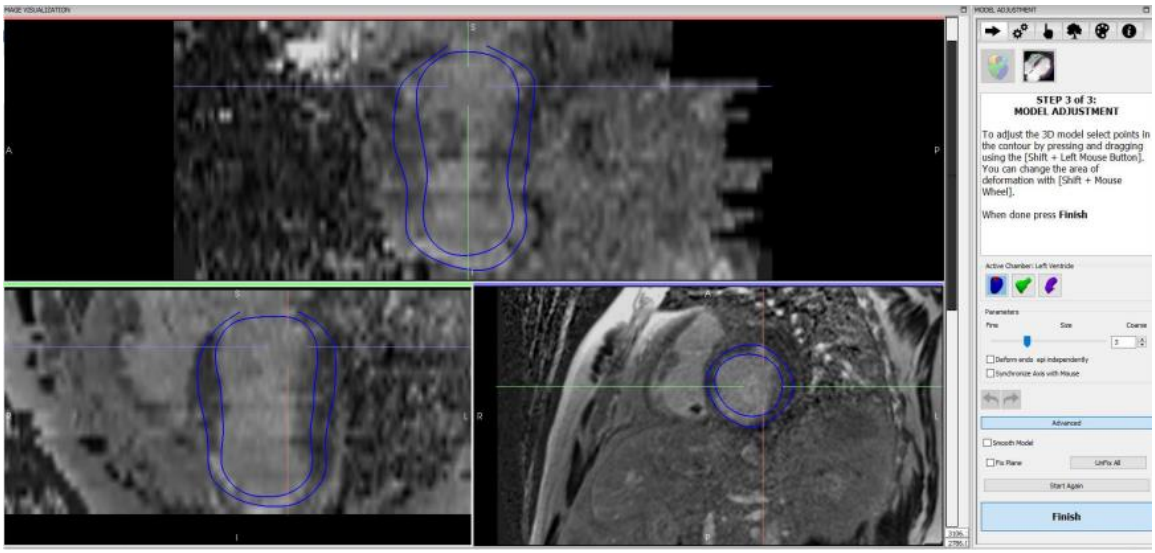

Figure 20: Model adjustment interface, final step of segmentation in ADAS-3D.

Depending on how large the deformation to be performed in each case, it is necessary to choose a certain deformation size. In the most delicate areas, a low deformation size should be chosen.

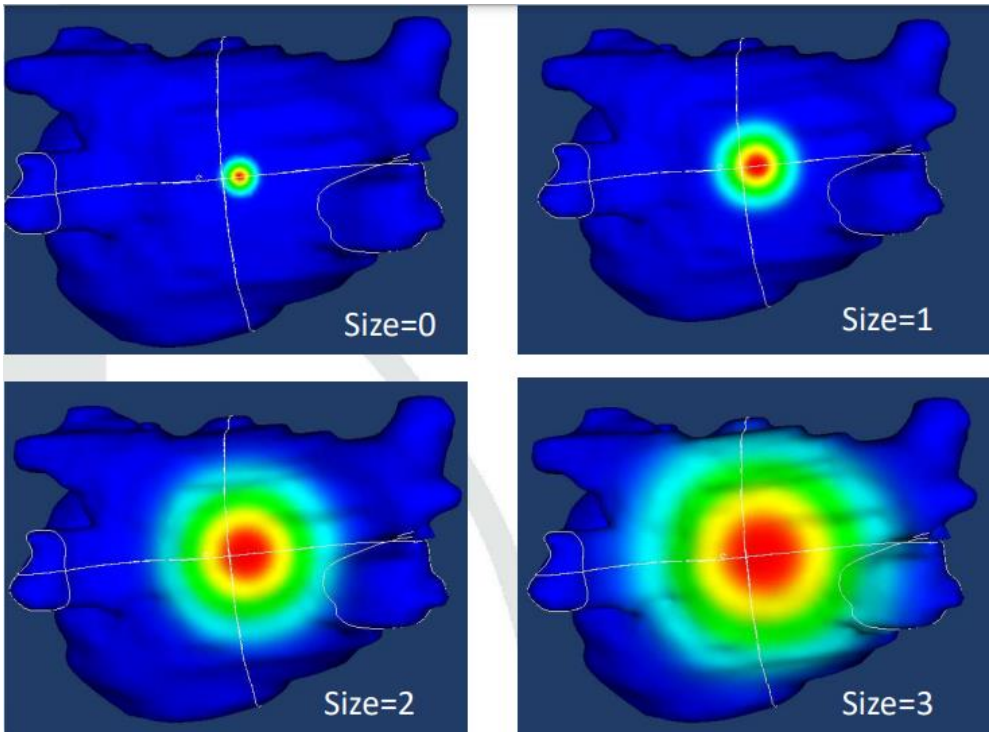

Figure 21: Scale of deformation sizes in model adjustment.

5.2.3.3. Review

Once the whole segmentation process is finished, a three-dimensional representation of the LV is obtained by layers of tissue thickness depth.

Before proceeding to adjust the thresholds in order to extract information from the model, I have considered it necessary to review all the cases since the segmentation process constitutes a very large dependent variable for study that has a considerable impact on the final results.

1. Checking segmentation

The first thing I have done is to go over each case again, checking that the contours defined during segmentation adapt correctly to the shape of the LV in each of the layers, having to deform the perimeter when necessary, on the model adjustment tool.

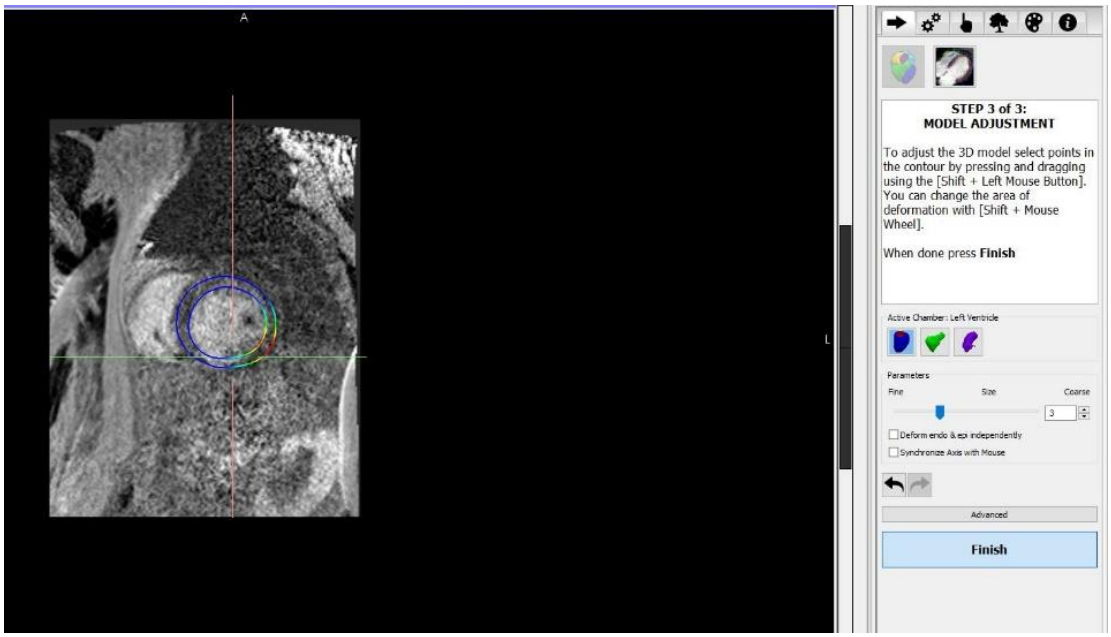

Figure 22: Model adjustment interface. Tool used in the revision of the segmentations layer by layer.

2. Excluding invalid areas

In some of the MRI, artifacts that cause noise have been observed. This noise generates areas of excessive brightness in regions where the pixel intensity would be lower if the artifact did not exist, causing that what is observed in that area does not correspond to the real characteristics of the substrate.

This factor causes a disturbance when the program classifies the substrate into healthy tissue, core and BZ (where the CCs circulate). This is because the criterion used by the program to carry out this classification is the brightness intensity. The more intense a zone is (the brighter it is), the more gadolinium the tissue has absorbed and, therefore, the more hypoxia it presents. To perform this classification, the program averages the brightness intensity of all the pixels in the area delimited between the endocardium and the epicardium, and then sets two values to act as thresholds for classifying the tissue according to its nature. Therefore, noise causes a distortion in the mean brightness intensity that disturbs the correct tissue representation automatically performed by the program.

2.1. Artifact classes

For the correct development of the project, it is essential to know how to detect and recognize all the causes that can generate noise, both artifacts and areas that can induce an error of interpretation by the program.

The main artifacts that I have observed have been the following:

- Artifact originated by the presence of an ICD. It should be taken into account that most of the patients in this study have an ICD implanted because the 2D MRI imaging technique is usually used in patients with this device. This is because 3D MRI, which has higher quality, is not used for patients with these characteristics because the ICD causes an even greater disturbance in the image.
- Artifact due to the appearance of anatomical structures in the plane that overlap the ventricular tissue. The clearest example is the valves.

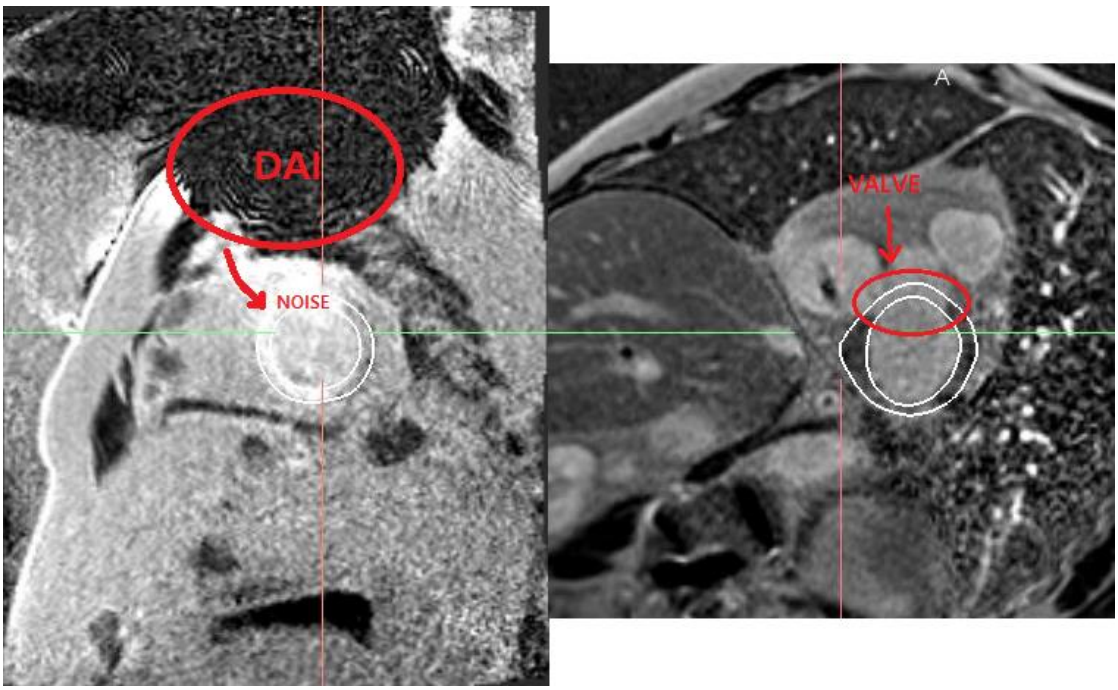

Figure 23: Types of artifacts. Left: Caused by an ICD. Right: Presence of the aortic valve.

2.2. Noise removal

To solve this drawback, the ADAS-3D program has an option that offers the possibility to exclude certain areas from the study it makes to identify the substrate. The excluded areas provide information about the anatomical shape of that region, but do not provide information about the brightness intensity in that region, so it will not affect the computation of the overall mean brightness intensity and the tissue characteristics in that region will not be represented.

In this way, the areas with noise are prevented from affecting the method used by the program to classify the tissue, achieving a more accurate identification of the substrate.

To perform this step, I have gone layer by layer selecting with the cursor the regions affected by noise that I wanted to exclude.

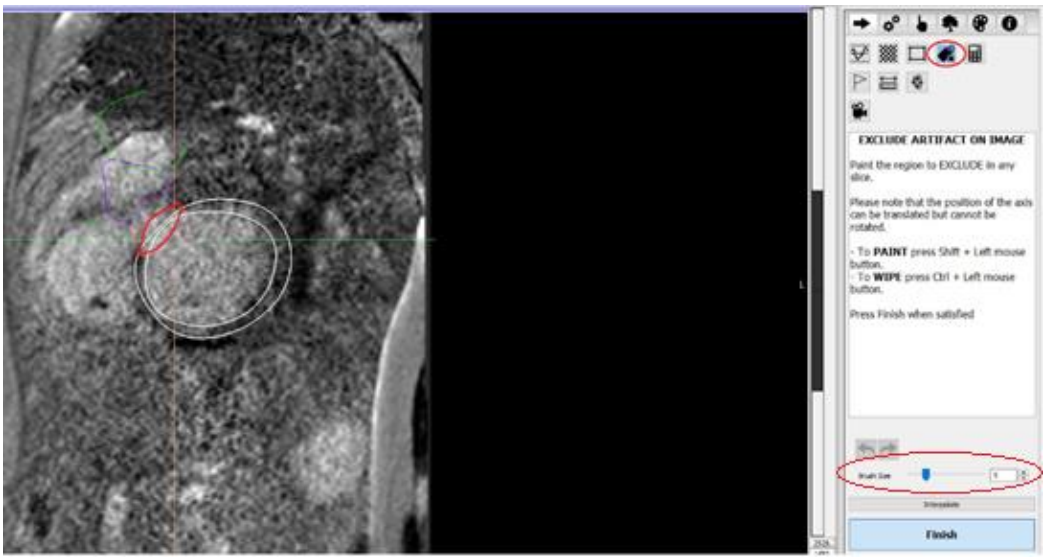

Figure 24: Screen showing the tools to exclude non-valid zones.

5.2.3.4. Visualization of the 3D LV model

Finally, we obtain a three-dimensional representation of the patient's LV.

The colour is related to the brightness intensity in each region and depends on the set thresholds, which by default are 40% and 60%. This code means the following:

- Zone with brightness intensity comprised in the range of 60% to 100% (light areas) will have red colour and represent tissue with hypoxia.
- Zone with brightness intensity in the range of 40% to 60% (grey zones) will have the colour white and represent the BZ.
- Zone with brightness intensity in the range of 0% to 40% (dark zones) will have blue colour and will represent the healthy tissue.
- Zone excluded from totally white colour.

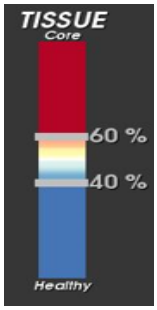

Figure 25: Colour code of the 3D map of the LV. Obtained from the study.

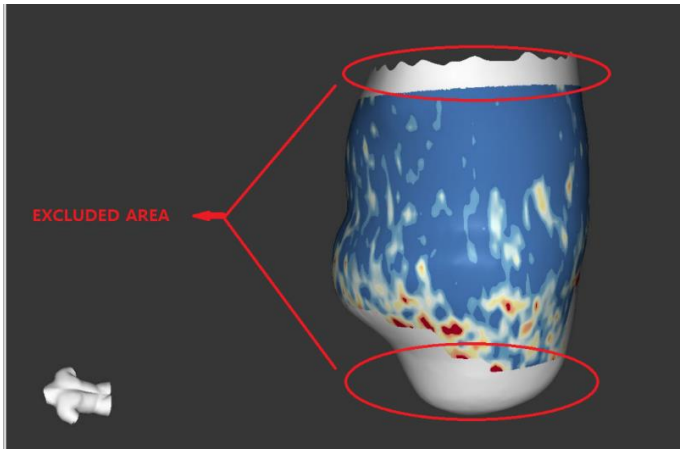

Figure 26: Example of a LV 3D model. Excluded zones are marked.

The ADAS-3D interface allows us to see the LV in several planes at the same time and also allows us to rotate in the three axes of space the representation of the LV to see it from different angles.

In addition, it is also able to show us the ventricular substrate at different levels of depth of tissue thickness. It divides this measurement into 9 layers ranging from the endocardium (10%) to the epicardium (90%).

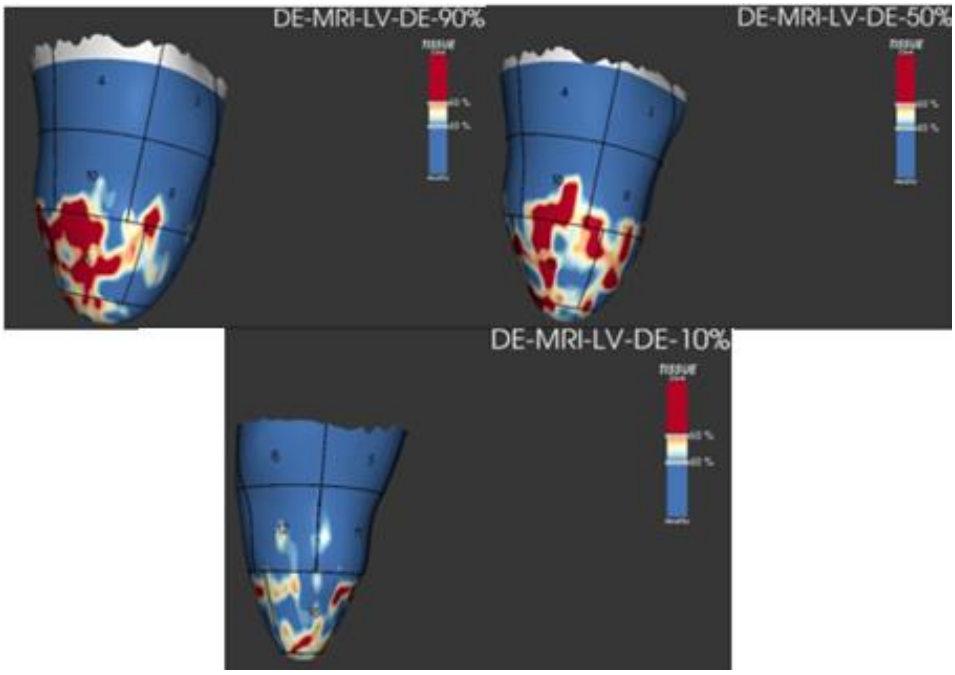

Figure 27: Visualization of the LV in different layers. Up-Left: Epicardium. Up-Right: Intermediate layer. Down: Endocardium.

5.2.4. Threshold adjustment

Once the LV of the patient in question was segmented and represented, I had to adjust the brightness thresholds to ensure that each region of the substrate was correctly identified.

The MAG reconstruction sequence has already established approximate brightness thresholds that make the representation assimilate to reality. These are 40-60% as a general rule, although they may vary depending on the case. For this reason, the threshold settings of all MAG samples have been checked and calibrated by my tutor Paz Garré, a professional specialist in this field.

Next, I have performed a very valuable phase of the work, as it responds to one of the main objectives of the project: to determine the brightness intensity threshold that adequately characterizes the ventricular substrate for images obtained using the PSIR reconstruction sequence.

To develop this part the first step consists of opening the MAG reconstruction of a patient in which the thresholds are correctly defined. The second step consists of opening the PSIR reconstruction of the same patient and modifying the lower and upper threshold until the representation is as similar as possible to the one obtained by the MAG sequence.

To facilitate the task, I have divided the LVs into AHA segments, which is a system that divides the ventricular surface into 17 sections that are in an exact position. Thus, it has been easier for me to control the position in which both models are located to make the comparison. It should also be noted that both models must be represented in the same layer.

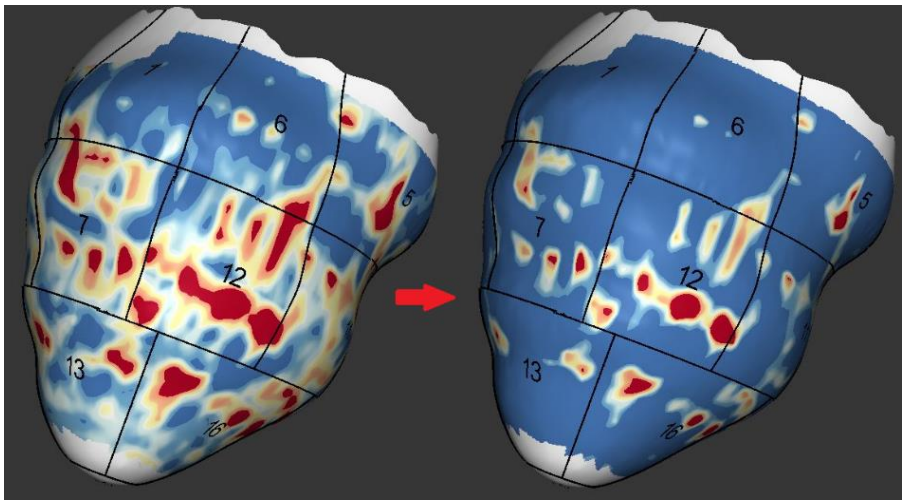

Figure 28: Image comparing before and after adjusting the thresholds. Left: before. Right: after.

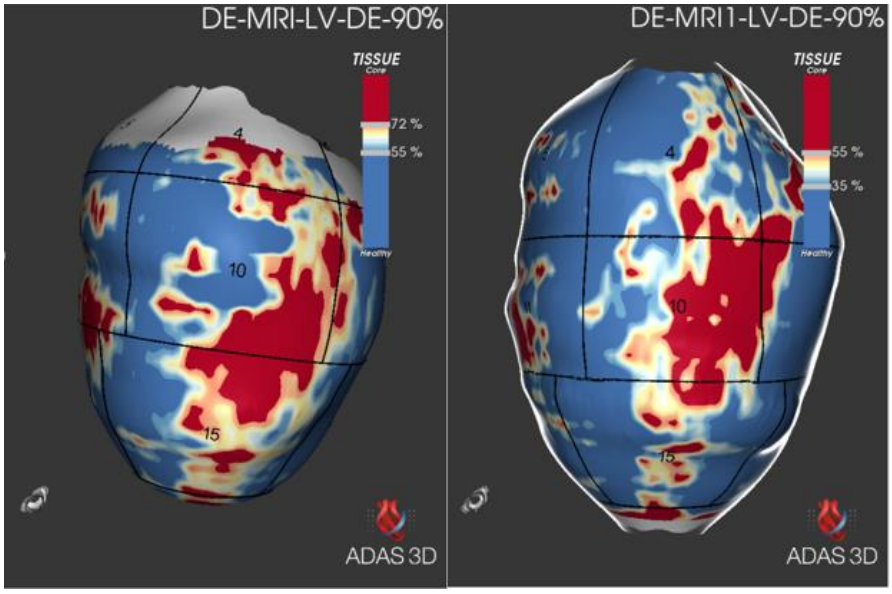

Figure 29: Image comparing a PSIR model with a MAG model once the thresholds have been adjusted. Left: PSIR. Right: MAG.

5.2.5. Database creation

At this point I have, for each patient, two segmented ventricular representations with correctly set thresholds, one representation formed by images reconstructed with the MAG sequence and the other formed by images reconstructed with the PSIR sequence.

It is time to collect objective information useful to compare both reconstruction sequences and to determine the level of validity of the PSIR sequence. In the clinical setting, the main purpose of these image processing techniques is to determine and localize in the ventricular substrate the

CC ls causing the TV, in order to be able to intervene. For this reason, this project has focused on comparing and validating this aspect. So, the information I need must be related to these CCs.

5.2.5.1. Feature selection

The ADAS-3D software has been a very useful resource for the project because it has a program that automatically detects arrhythmogenic channels by analysing the 3D structure of the model. In addition, they are represented in the 3D model of the LV and the layers through which each of the CCs passes are indicated.

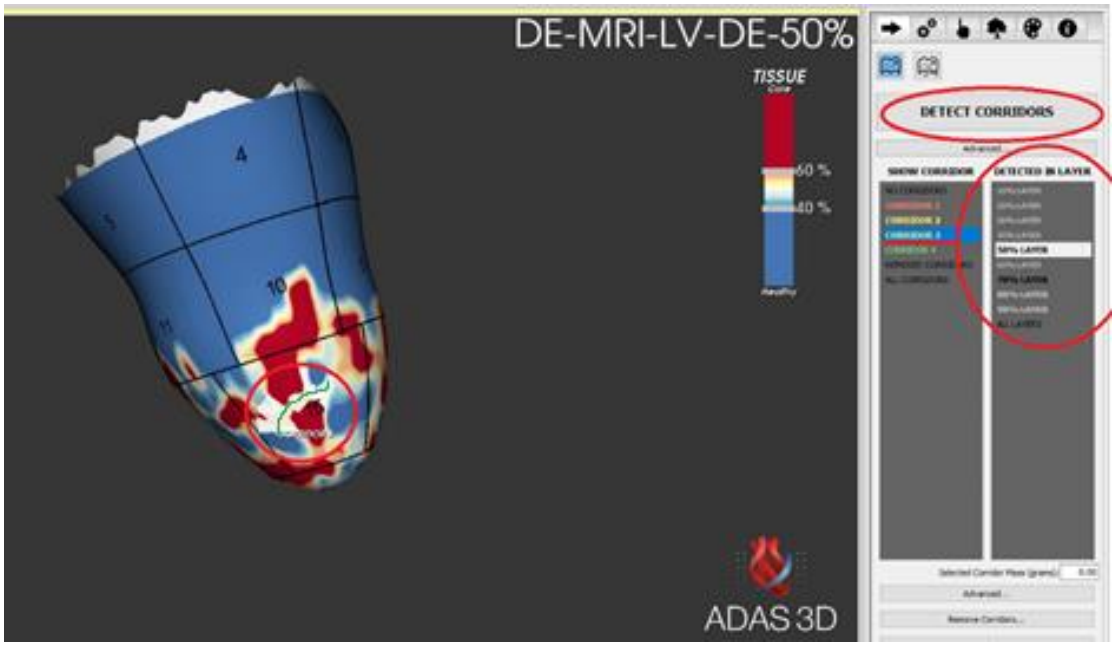

Figure 30: Screen showing the location and information given by the program about the detected channels. Channel highlighted in green.

On the other hand, there is also an option that calculates a large number of data that provide descriptive information on a large number of characteristics. From all the information provided by the program I have chosen the following variables:

- Value of the set thresholds, lower and upper, for the correct identification of the substrate(%).
- Number of CCs detected by the program
- Position of each CC by AHA zones
- Position of each CC by depth layers
- Mass of each CC

  For each AHA segment in each layer:

  - Total area of the zone(cm^2)
  - Area of BZ and Core(cm^2)
  - Percentage of BZ and Core(%)
  - BZ Area(cm^2)

- Percentage of BZ(%)
- Core Area(cm^2)
- Percentage of Core(%)

From these variables, other parameters could also be obtained:

- average CC mass=total mass of CCs / number of CCs
- healthy area = total area of the zone - area of BZ and core

The reason why I have chosen these parameters is because they describe in a very valuable, objective and accurate way the structure and composition of the substrate shown by each model. In addition, they also provide effective information about the CCs and their determination by sections and layers.

5.2.5.2. Feature extraction

To extract all the necessary parameters for the comparative study I have first had to create a database in SPSS containing the patient identification number, the reconstruction sequence used (MAG or PSIR) and all the variables of the parameters to be collected.

Finally, I had to consult all the models, check the information about the detected CCs and click on the *Statics* option, which calculates all the data of interest, and write down the values in the database until it was complete.

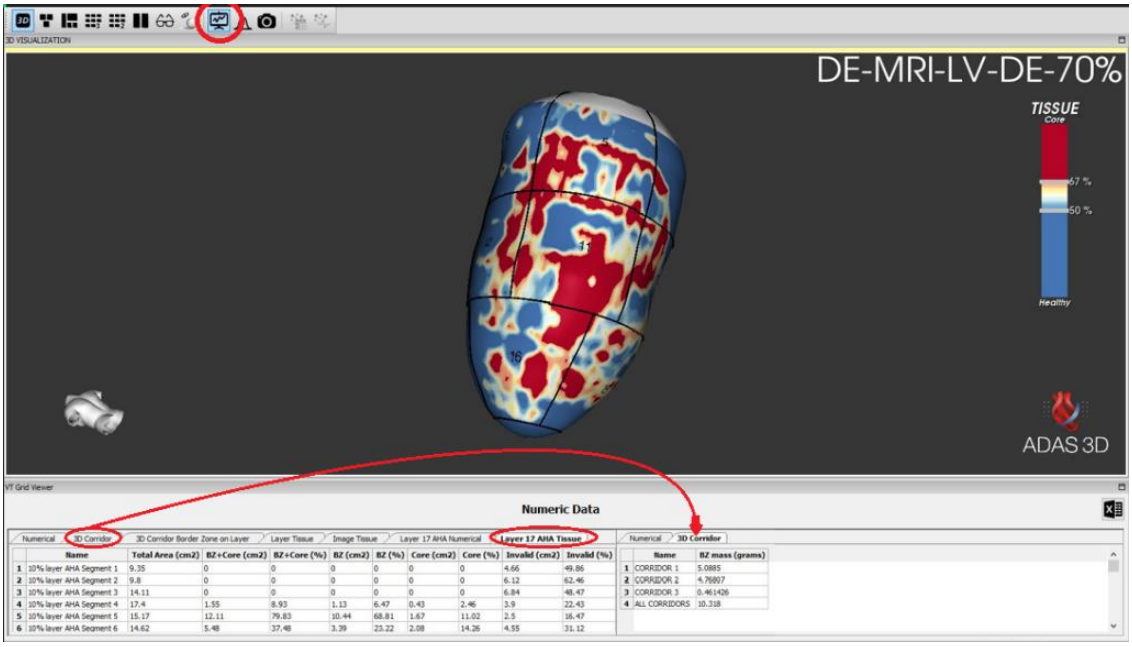

Figure 31: Screen showing where the data relating to the parameters characterizing the channels and the tissue are obtained from.

5.2.6. Statistical analysis

After collecting as much data as possible that could provide information on the ventricular substrate, I selected the characteristics that could be useful for achieving the objectives set and developed a statistical approach.

First, I had to restructure the database to facilitate the work of statistical analysis. In this part, I reduced the number of study parameters, because I had too many data, and I modified the format of the database in SPSS in order to reduce the number of variables.

One of the objectives of the project is to determine the range of threshold values that make the ventricular model as representative as possible. To achieve this, I have required the values in relation to this aspect that I have been annotating throughout the process of fitting the thresholds with each of the cases. Then, using the SPSS and RStudio, I calculated a set of measures to clarify this question.

The other major objective is to validate the PSIR sequence using the MAG sequence as a reference. To do this, I decided that it was convenient to compare and perform a similarity study of several descriptive parameters. On the one hand, I compared the number and total mass of the channels detected in each case. On the other hand, I compared the area of healthy, fibrotic and BZ tissue identified by ADAS-3D in each of the AHA segments corresponding to the 10%, 50% and 90% layers of each ventricle studied. I have decided to take into account only these 3 layers of ventricular tissue thickness because they provide a general characterization of the tissue, since they correspond to the endocardium, mesocardium and epicardium region. Once the database had been restructured, with the SPSS and RStudio I have performed a linear correlation study based on coefficients and statistical tests.

5.3. Results

DETERMINATION OF CONTRAST THRESHOLDS FOR PSIR

The first part of the statistical study has focused on analysing the upper and lower threshold contrast values set on all samples and defining which values allow the optimal representation for PSIR sequenced images.

It is important to remember how the contrast setting works: regions with brightness intensity below the lower threshold are identified as healthy tissue (blue), regions with brightness intensity above the lower threshold and below the upper threshold are identified as BZ tissue (white) and regions with brightness intensity above the upper threshold are identified as core tissue (red). The threshold value corresponds to a percentile of the set of pixel intensity values that the segmented region has.

	Reconstruction sequence	*N*	*Mean*	*Standard deviation*	*Standard error*
Lower threshold	MAG	21	37,8571	8,49874	1,85458
	PSIR	21	60,5714	7,58005	1,6541
Upper threshold	MAG	21	55,9524	7,57282	1,65253
	PSIR	21	72,4762	6,99728	1,52693

Table 2: Table showing the results of the statistical study of the contrast thresholds. Statistical indicators: mean, sd and se.

The arithmetic mean of the threshold values used to adjust the contrast in each case has been calculated for the MAG and PSIR samples. This measure means a representative value for the variable, that is, the expected value of the variable.

On the other hand, we can also know the standard deviation and the standard error of the sample. The standard deviation indicates how scattered the data is around the mean and the standard error indicates how the mean can vary depending on the sample chosen to calculate it.

The results obtained, calculating the mean, confirm that the thresholds that favour a representative visualisation are 37.85 ± 1.85 and 55.95 ± 1.65.

Analysing the other reconstruction sequence, the data have shown that the thresholds that favour a representative visualisation of the PSIR images are 60.57 ± 1.65 and 72.48 ±- 1.52, on average. We can also see that there is a standard deviation of 7.58 for the lower threshold and 7.00 for the upper threshold.

	Levene's test for equality of variances		**T test for equality of means**				
	F	*Sig.*	*t-value*	*dof*	*p-value (bilateral)*	*Mean difference*	*St. error of the difference*
Lower threshold	0,334	0,566	-9,14	40	0	-22,71429	2,48506
Upper threshold	0	0,994	-7,344	40	0	-16,52381	2,24997

Table 3: Table showing the results of the student's t-test for difference of means on the data corresponding to the contrast thresholds.

Next, a hypothesis test for difference of means was performed. This test consists of comparing a variable, which in this case was the upper and lower threshold, in two different groups or samples, which in this case was MAG and PSIR. The purpose is to find out whether the variable being analysed has a similar behaviour in both groups. Firstly, we must bear in mind that the samples of thresholds in MAG and PSIR do not depend on each other, therefore, they are independent samples.

To be able to carry out this test, it is necessary to check that the variance of the two groups is homogeneous, this is because in order to determine whether the two samples are equal, the mean of one must be able to be projected onto the variability of the other. For this purpose, Levene's test is applied, in which the null hypothesis states that the variances are equal and the alternative hypothesis states that they are not. The resulting significance level is 0.57 for the lower threshold and 0.99 for the upper threshold. As they exceed the academically defined significance margin of 0.05, the null hypothesis that states the homogeneity of variances between the two groups is accepted and, therefore, means that the requirements for the student's t-test for difference of means are met.

In the T-student test for difference of means, we have a null hypothesis that states that the means of MAG and PSIR thresholds are equal or similar and an alternative hypothesis that negates it and states that the means are not equivalent. This test calculates a t-value from the means and variances of the two groups. The t-value measures the size of the difference in relation to the

variance in the sample data, it is simply the calculated difference represented in standard error units.

$$T - value = \frac{\text{mean MAG} - \text{mean PSIR}}{\sqrt{(\frac{\text{sdMAG}}{\text{nMAG}} + \frac{\text{sdPSIR}}{\text{nPSIR}})}}$$

Equation 1: T-value formula. sd: standard deviation. n: sample's size.

From the t-value and the degrees of freedom of the sample, taking into account that the data follow a normal distribution, we obtain the p-value, which determines whether the difference in the means of both sequences is statistically significant and not due to chance.

In this particular case, we have obtained a t-value of -9.140 for the lower threshold and -7.344 for the upper threshold, which generates a p-value of 0.000 for both thresholds. As the p-value is less than 0.05, the results fall within the confidence interval, which is 95%. Therefore, the null hypothesis is rejected, confirming that the means of the two groups are different and have no similarity.

It also indicates that the difference in means between the two sequences is 22.71 for the lower threshold and 16.52 for the upper threshold. The PSIR thresholds are higher.

VALIDATION OF DATA OBTAINED FROM PSIR

The other main objective of the project is to compare the characterisation of channels and ventricular tissue provided by ADAS-3D with both sequences to determine their degree of similarity. To this end, the following variables have been studied: number of channels detected, total mass of channels detected, area of healthy tissue identified, area of BZ tissue identified and area of core tissue identified.

CHANNEL CHARACTERIZATION

Number of channels detected

To study these variables, firstly, a scatter plot has been shown to represent the values of the characteristic in question for MAG and PSIR. This graph can visually suggest the type of correlation that exists between the two sequences.

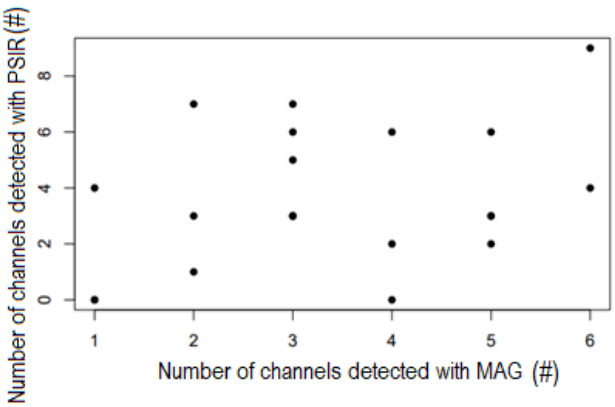

Figure 32: Scatter plot of number of channels detected

Regarding the number of channels detected, we can observe that the scatter plot shows an extremely weak correlation (almost non-existent), with a very slightly positive trend.

```
##  Pearson's product-moment correlation
##
## data:  dades_2$N_CC_mag and dades_2$N_CC_psir
## t = 1.583, df = 19, p-value = 0.1299
## alternative hypothesis: true correlation is not equal to 0
## 95 percent confidence interval:
##  -0.1059431  0.6737581
## sample estimates:
##       cor
## 0.3413553
```

Next, we intend to measure the correlation between both groups in order to understand the degree of association they have for each characteristic. To do this, the Pearson's product moment is calculated with RStudio, which measures the strength and direction of the association between the two variables. The test analyses the significance level using the T-student contrast. It assumes that both variables are independent of each other and have a normal distribution.

The measure analysed in this T-student test is the correlation coefficient r, which is obtained from the covariance of the two variables divided by the product of their standard deviation. It ranges from -1 to 1, which corresponds to a perfect negative correlation and a perfect positive correlation, respectively, considering r=0 as a result of no correlation.

$$r = \frac{n \cdot (\sum varMAG \cdot varPSIR) - (\sum varMAG) \cdot (\sum varPSIR)}{\sqrt{[n \cdot \sum varMAG^2 - (\sum varMAG)^2] \cdot [n \cdot \sum varPSIR^2 - (\sum varPSIR)^2]}}$$

Equation 2: Pearson's product moment correlation formula. n: sample's size. var: value of the variable.

We set as null hypothesis that there is no association between the two sequences, because we assume that one variable does not depend on the other. If the null hypothesis is satisfied, the value of r would be 0. However, for a random data set, r may be non-zero, but close to zero. Therefore, we must define how much the correlation coefficient r can differ from 0 so that the result is not due to chance. When implementing the T-student test, we obtain a t-value, which, in this case, is calculated by knowing the value of r and the population size (n).

$$t = \frac{r \cdot \sqrt{n-2}}{\sqrt{1-r^2}}$$

Equation 3: t-value formula for regression

Consequently, the p-value is calculated, which represents the statistical significance level of the test and gives us the probability that the association between the two variables is due to chance. Therefore, the smaller the p-value, the better. Conventionally, this value is set at 0.05, so that if the p-value is lower than these values, we can consider the association between the variables to be statistically significant. We should bear in mind that this method is sensitive to outliers, those points that are too far away from the others, so they can alter our result.

Looking at the results obtained from the Pearson product moment correlation, we see that the r is 0.34, which could mean a slight correlation with a positive slope. However, if we look at the p-value, 0.1299, we see that this is greater than the limit we have defined of 0.05, so we can consider that the slight correlation we see is due to chance and that it has no meaning in statistical terms. The scatter plot already shows that there is no clear relationship.

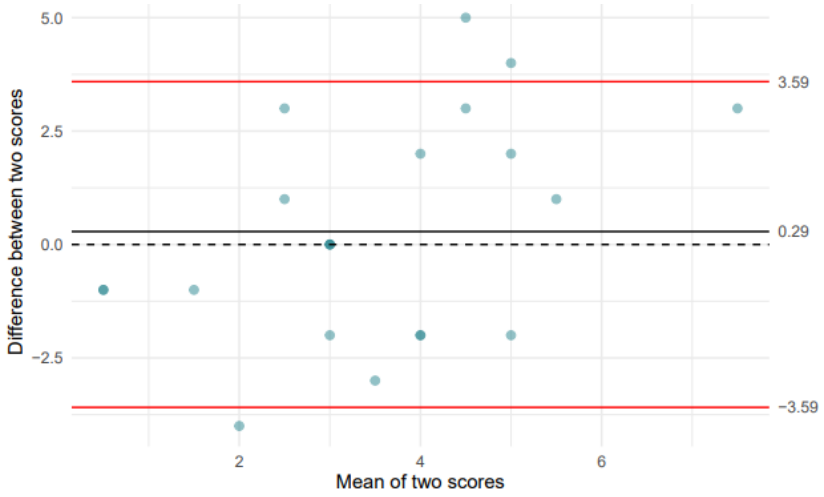

Figure 33: Band Altman Change Plot of Number of channels detected

Next, the Bland-Altman method has been applied, a graphical method, widely used in biomedical and biochemical literature, which allows the comparison of two measurement techniques, MAG and PSIR, on the same quantitative variable, in this case the number of channels detected. It is applicable to cases where it is necessary to measure the difference between a new method and an established one, in order to validate or not the new one, depending on whether it is reliable and reproducible for the intended use. For this purpose, the Bland-Altman method quantifies the mean difference between the two methods (bias) and a confidence range, which is expected to include 95% of the differences in values obtained by MAG and PSIR.

In this representation, the Y-axis corresponds to the differences between the particular values obtained by MAG and PSIR [var MAG - varPSIR]. The X-axis represents the respective mean value of both [(var MAG var PSIR)/2].

The three parallel lines represent:

- Upper limit of agreement: mean difference + 1.96-sd
- Mean difference or bias: mean of the difference in means between the two sequences
- Lower Limit of agreement: mean difference - 1.96-sd

The bias is a measure of the accuracy of the measurement system and represents the systematic error of the new method to be validated, namely PSIR. If MAG and PSIR obtain similar values on average, then the bias will be close to zero. If it is far from this value, it means that the two methods produce different results.

The representation of the limits of agreement allows to visually judge the agreement between the two methods. These limits establish the range of values in which the difference between the two

techniques will lie 95% of the time. The smaller the range between the limits, the better the agreement. A high range between both limits of agreement would imply a low accuracy of the non-validated method, PSIR.

Regarding the plotted data, it is important to observe if the variability is constant over the range of values and around the mean difference line, or if anomalies are detected, for example: the data around the bias line follow a certain trend as the value of the mean between the two techniques increases or the majority of the data are above or below this line.

As for the number of channels, it can be seen that it has a bias of 0.29, which means that, on average, PSIR detects 0.29 channels less than MAG. It also has limits of ±3.59, which means that, in 95% of the cases, the channels detected by PSIR can be discerned in 3 or 4 units. The values do not follow any particular evolution in the graph, they are chaotic and are found both above and below the bias.

```
##         est       lower     upper
## 1 0.3041825 -0.08181811 0.6108309
```

Finally, the concordance correlation coefficient, which estimates the degree of agreement of a continuous measure obtained by two different methods, is calculated with RStudio.

$$\rho = \frac{2 \cdot s(MAG, PSIR)}{sMAG^2 + sPSIR^2 + (meanMAG - meanPSIR)^2}$$

Table 4: Formula for the correlation coefficient of concordance. s(x,y): covariance. $s(x)^2$: variance.

It is used to assess reproducibility or inter-rater reliability. The higher it is, the greater the degree of correlation between the two variables. The following table is used as a reference to determine the degree of concordance.

Concordance degree	**ρ**
Near perfect	> 0,99
Substantial	0,99 - 0,95
Moderate	0,95 - 0,9
Poor	< 0,9

Table 5: Table of interpretation of the concordance correlation coefficient. Extracted from: https://www.scielo.sa.cr/scielo.php?script=sci_arttext&pid=S0001-60022008000400005

The correlation coefficient of agreement is 0.304, which shows that in this aspect PSIR has a very poor agreement with MAG.

Total mass of detected channels

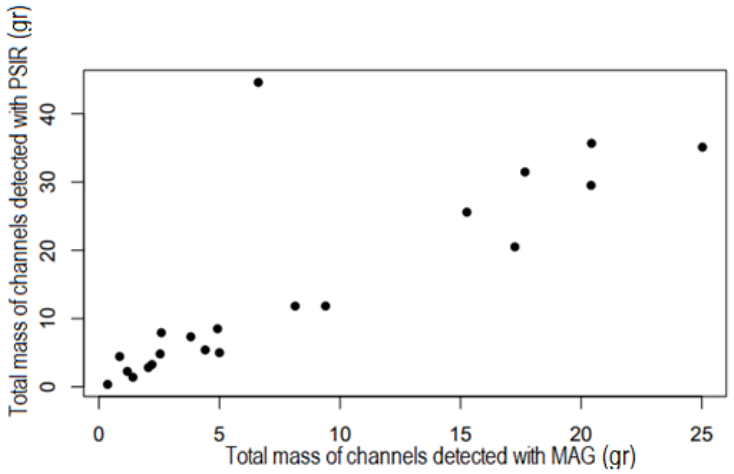

Figure 34: Total mass of detected channels scatter plot

In this feature, we can see that the scatter plot shows a considerable correlation with a positive trend.

```
##  Pearson's product-moment correlation
##
## data:  dades_2$MASS_mag and dades_2$MASS_psir
## t = 6.157, df = 19, p-value = 6.445e-06
## alternative hypothesis: true correlation is not equal to 0
## 95 percent confidence interval:
##  0.5936347 0.9227446
## sample estimates:
##       cor
## 0.816167
```

Looking at the results obtained from the Pearson product moment correlation, we see that the r is 0.82, which could mean a strong correlation with a positive slope. If we look at the p-value, 6.445e-06, we see that this is lower than the limit we have defined of 0.05, so we can consider that the correlation we see is not due to chance and that it does have meaning in statistical terms.

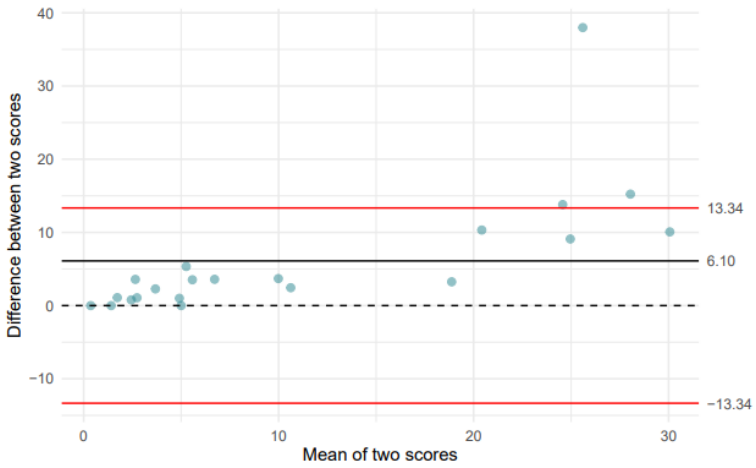

Figure 35: Band Altman change plot of total mass of channels detected

As for the total mass of the channels, it can be seen that it has a bias of 6.10, which means that, on average, PSIR detects 6.10 grams less total mass of channels than MAG. It also has limits of ±13.34, which means that, in 95% of the cases, the total mass of channels detected by PSIR can discern 13.34 grams. The values do not follow any particular evolution in the graph and are above the bias.

```
##         est     lower     upper
## 1 0.6057132 0.3794456 0.7636164
```

The correlation coefficient of concordance is 0.605, which shows that in this aspect PSIR has a poor concordance with MAG.

TISSUE CLASSIFICATION AND QUANTIFICATION

Area of healthy tissue

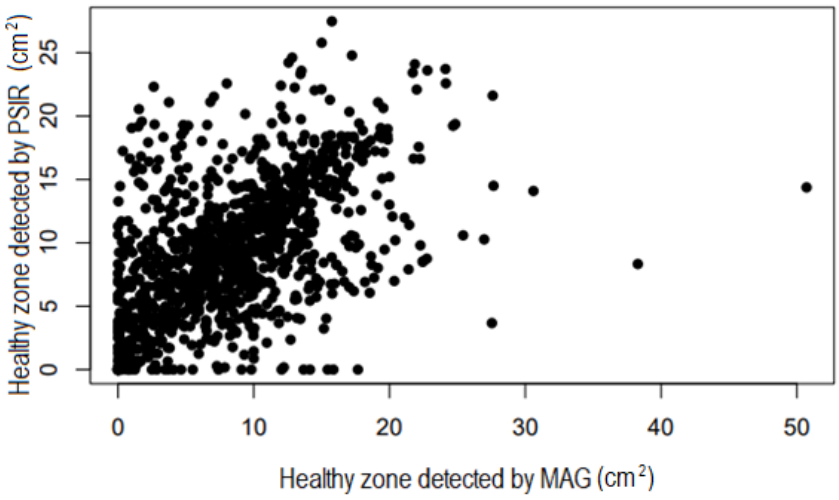

Figure 36: Healthy tissue area scatter plot

In this feature, we can see that the scatter plot shows a considerable correlation, with a positive trend.

```
##  Pearson's product-moment correlation
##
## data:  dades_1$HEALTHY_AREA_mag and dades_1$HEALTHY_AREA_psir
## t = 20.361, df = 1069, p-value < 2.2e-16
## alternative hypothesis: true correlation is not equal to 0
## 95 percent confidence interval:
##  0.4840484 0.5704610
## sample estimates:
##       cor
## 0.5286229
```

Looking at the results obtained from the Pearson product moment correlation, we see that the r is 0.53, which could mean a moderate correlation with a positive slope. If we look at the p-value, 2.2e-6, we see that this is less than the limit we have defined of 0.05, so we can consider that the correlation we see is not due to chance and that it does have meaning in statistical terms.

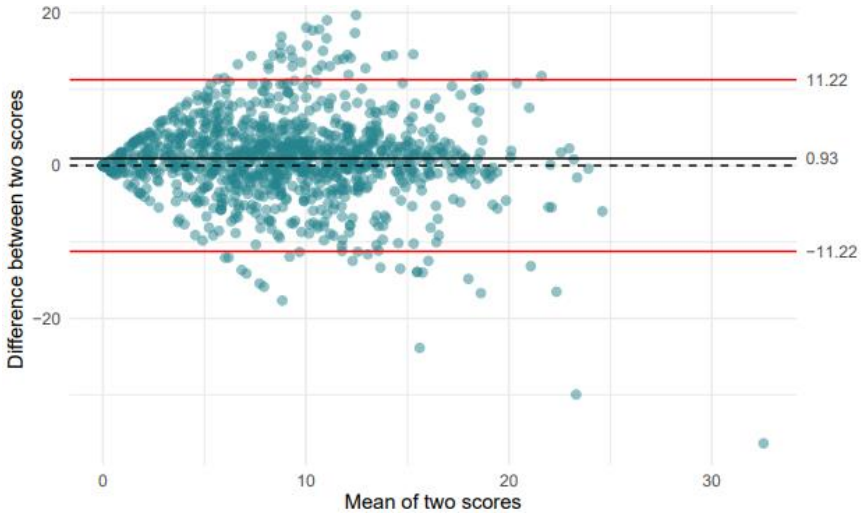

Figure 37: Band Altman change plot of healthy tissue area

As for the healthy tissue area, it can be seen that it has a bias of 0.93, which means that, on average, PSIR detects 0.93 cm^2 less healthy tissue than MAG. It also presents limits of ±11.22, which means that, in 95% of the cases, the healthy area detected by PSIR can discern 11.22 cm^2. We can also see that as the mean of the measurements increases, the difference between them also increases, which means that the higher the value of the variable, the more inaccurate PSIR is. The values are both above and below the bias.

```
##         est     lower     upper
## 1 0.5200989 0.4757408 0.5618182
```

The correlation coefficient of concordance is 0.52, which shows that in this aspect PSIR has a poor concordance with MAG.

Area of BZ tissue

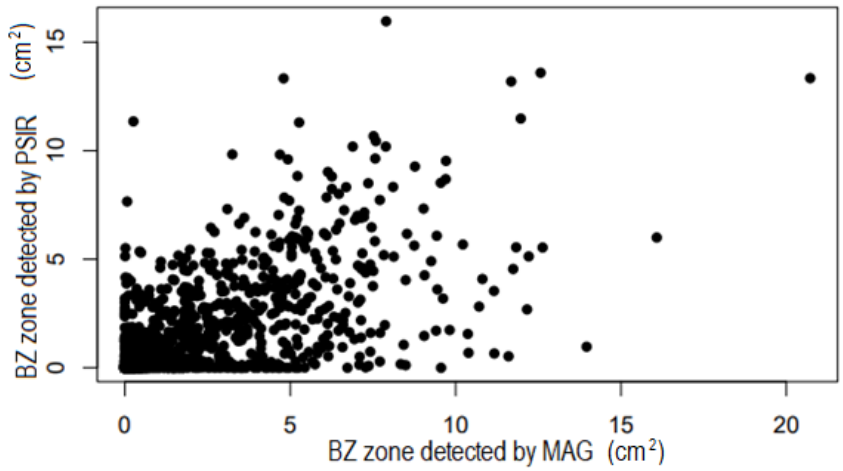

Figure 38: Scatter plot of BZ tissue zones

In this feature, we can observe that the scatter plot shows a weak correlation, with a positive trend.

```
##  Pearson's product-moment correlation
##
## data:  dades_1$BZ_AREA_mag and dades_1$BZ_AREA_psir
## t = 24.115, df = 1028, p-value < 2.2e-16
## alternative hypothesis: true correlation is not equal to 0
## 95 percent confidence interval:
##  0.5605922 0.6387237
## sample estimates:
##       cor
## 0.6010923
```

Looking at the results obtained from the Pearson product moment correlation, we see that the r is 0.60, which could mean a moderate correlation with a positive slope. If we look at the p-value, 2.2e-6, we see that this is lower than the limit we have defined of 0.05, so we can consider that the correlation we see is not due to chance and that it does have meaning in statistical terms.

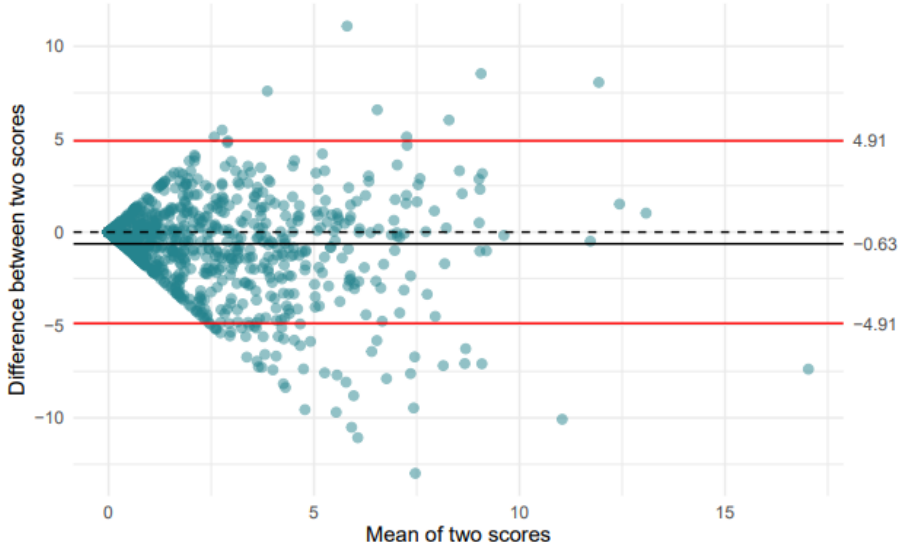

Figure 39: Band Altman change plot of BZ tissue area

As for the area of BZ tissue detected, it can be seen that it has a bias of -0.63, which means that, on average, PSIR detects 0.63 cm^2 more BZ tissue than MAG. It also presents limits of ±4.91, which means that, in 95% of the cases, the BZ tissue identified by PSIR can be discerned in 4.91 cm^2. We can also see that as the mean of the measurements increases, the difference between them also increases, which means that the higher the value of the variable, the more inaccurate PSIR is. The values are both above and below the bias.

```
##       est     lower     upper
## 1 0.576082 0.5357143 0.6138224
```

The correlation coefficient of concordance is 0.57, which shows that in this aspect PSIR has a poor concordance with MAG.

Area of core tissue

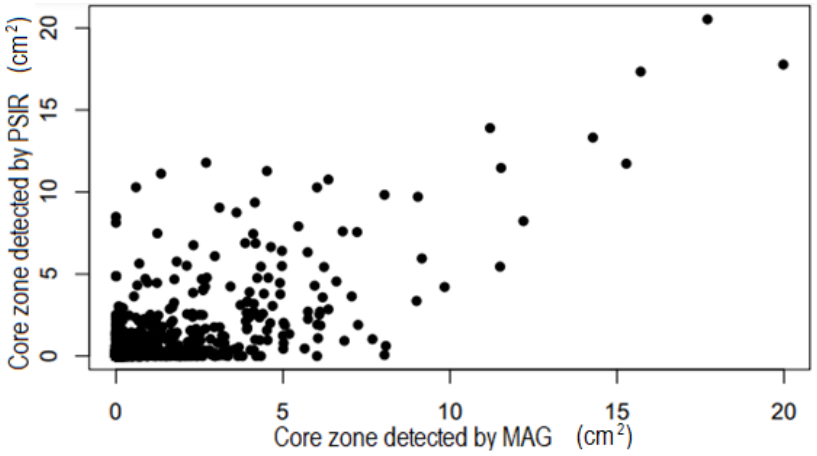

Figure 40: Scatter plot of core tissue area

In this feature, we can observe that the scatter plot shows a weak correlation, with a positive trend.

```
##  Pearson's product-moment correlation
##
## data:  dades_1$CORE_AREA_mag and dades_1$CORE_AREA_psir
## t = 34.608, df = 1028, p-value < 2.2e-16
## alternative hypothesis: true correlation is not equal to 0
## 95 percent confidence interval:
##  0.7040346 0.7605736
## sample estimates:
##       cor
## 0.7335708
```

When we look at the results obtained from the Pearson product moment correlation, we see that the r is 0.73, which could mean a considerable correlation with a positive slope. If we look at the p-value, 2.2e-6, we see that this is less than the limit we have defined of 0.05, so we can consider that the correlation that can be seen is not due to chance and that it does have meaning in statistical terms.

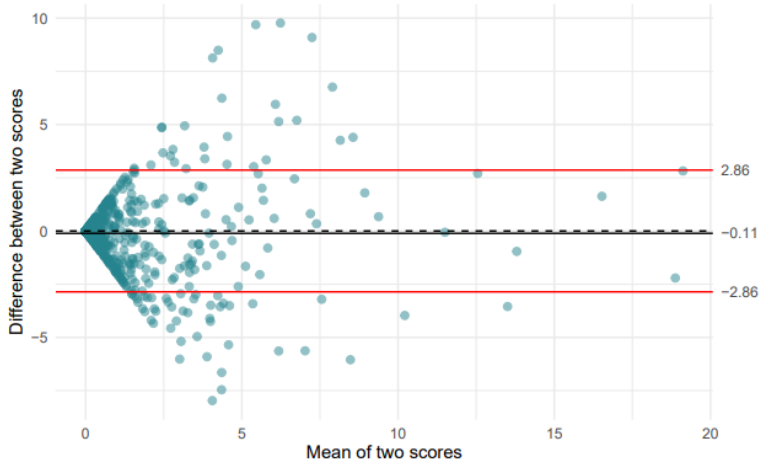

Figure 41: Band Altman change plot of core tissue area

As for the core area detected, it can be seen that it has a bias of 0.11, which means that, on average, PSIR detects 0.11 cm^2 of core area less than MAG. It also presents limits of ±2.86, which means that, in 95% of the cases, the core tissue detected by PSIR can be discerned in 2.86cm^2. We can also see that as the mean of the measurements of the variable increases, the difference between them also increases, which means that the higher the value of the variable, the more inaccurate PSIR is. The values are both above and below the bias.

```
##         est     lower     upper
## 1 0.7324307 0.7028465 0.7594856
```

The correlation coefficient of concordance is 0.73, which shows that in this aspect PSIR has a low concordance with MAG.

5.4. Discussion

When it comes to discussing the results, the same structure has been followed as in the previous section, where the results have been presented. Here, the data obtained from the statistical analysis will be interpreted and the information considered relevant to the project and which responds to the objectives set will be extracted.

Determination of contrast thresholds for PSIR

From the part in which the contrast thresholds that allow a representative visualisation of the ventricles, where the channels and types of tissues can be correctly appreciated, have been analysed, it has been possible to extract a great deal of information.

Thanks to the T-student test for mean difference, it has been demonstrated that the thresholds to be used in sequenced images with MAG and PSIR are not the same.

Also, it has been shown that the range conventionally used for MAG (40-60) is correct, since the analysis showed a similar average range, from 37.85 ± 1.85 to 55.95 ± 1.65, with a deviation close to 7 in both thresholds. This fact indicates that it is important to check the contrast during model processing, as there is some variation.

On the other hand, it has also been estimated that the optimal range of thresholds in the PSIR images is from 60.57 ± 1.65 to 72.48 ± 1.52, with a deviation similar to that of MAG.

In summary, we can conclude that, on average, in PSIR the lower threshold should be set 22.71 points above the optimal lower threshold for MAG and the upper threshold is usually 16.52 points higher. It should be emphasised that this conclusion is an approximation with limitations and that there is considerable variance in this parameter because it depends on each case.

Validation of data obtained from PSIR

In this part, the results have been interpreted independently for each variable studied. First the variables referring to the channels and then the variables referring to the identification of the ventricular tissue and measurement of its surface.

CHANNEL CHARACTERIZATION

For the characterisation of the channels detected in each case, the number of channels and their total mass were analysed.

With regard to the number of channels, it can be stated that this was the feature with the least correlation between the two sequences. Therefore, the weak point of the PSIR sequence is that of detecting the number of arrhythmogenic conduction channels in the patients, since the correlation index is 0.3, which means that there is no similarity with the MAG sequence in this aspect; they behave completely differently in relation to this variable. Moreover, on quite a few occasions, it can detect 4 channels above or below the correct ones (detected by MAG), which is a high degree of error, bearing in mind that 3-4 channels are usually detected per patient, on average.

On the other hand, PSIR is much more accurate in assessing the mass of arrhythmogenic channels, as the correlation is quite strong for this variable (r=0.82). In fact, it is the variable where the similarity for both techniques is higher. The bias is 6.10 grams, not too high considering that the total mass can be up to 35 grams, and the limits of agreement are not as high as with the previous variable, proportionally speaking. It has been found that in all cases MAG detects more mass than PSIR, since in the Band Altman diagram all the points are above 0 (meaning that the difference between the values of both sequences is always positive and , therefore, the value of MAG is always higher) and follow an upward trend. Thus, it could be concluded that PSIR tends to detect less mass.

TISSUE CLASSIFICATION AND QUANTIFICATION

For the identification and quantification of ventricular tissue, the area of healthy, BZ and fibrotic tissue was compared in both reconstruction techniques.

For all three tissue types, a moderate correlation of about r=0.6 was found. The calculations were represented in the diffusion diagrams, which showed considerably connected points forming an upward trend. However, several outliers were involved which may have influenced the results.

The Band-Altman plots showed small biases, small variances considering the range of values these variables can reach, and homogeneous behaviour. This means that the PSIR errors when evaluating these variables are not high and are only due to the size of the measurement, they do not follow any specific condition.

Tissue	**Healthy**	**BZ**	**Core**	**Mean**
Correlation coef.	0,53	0,56	0,73	0,61
Bias	0,93	0,63	0,11	0,56
Limit of agreement	11,22	4,91	2,86	6,33

Table 6: Table of statical results of ventricular types of tissues

Looking at the table with the summary of relevant results, it can be concluded that the more ischaemic the tissue, the more correlation there is between the two sequences and the more accurate PSIR is. This means that PSIR identifies core tissue more accurately than healthy

tissue, leaving BZ tissue in the middle. The BZ tissue is the most interesting tissue to study, as it is where the arrhythmogenic channels are usually located.

Therefore, it is corroborated that there is an evident correlation in these variables, although it is not a complete correlation. In addition, a relatively low overall bias of 0.56 is obtained, although the larger the measurement to be made, the more imprecise the PSIR sequence is. The validation of the PSIR sequence depends on the degree of acceptability that is deemed appropriate. In my opinion, the similarity should be higher to validate the sequence.

6. IMPLEMENTATION TIMELINE

6.1. Work breakdown structure

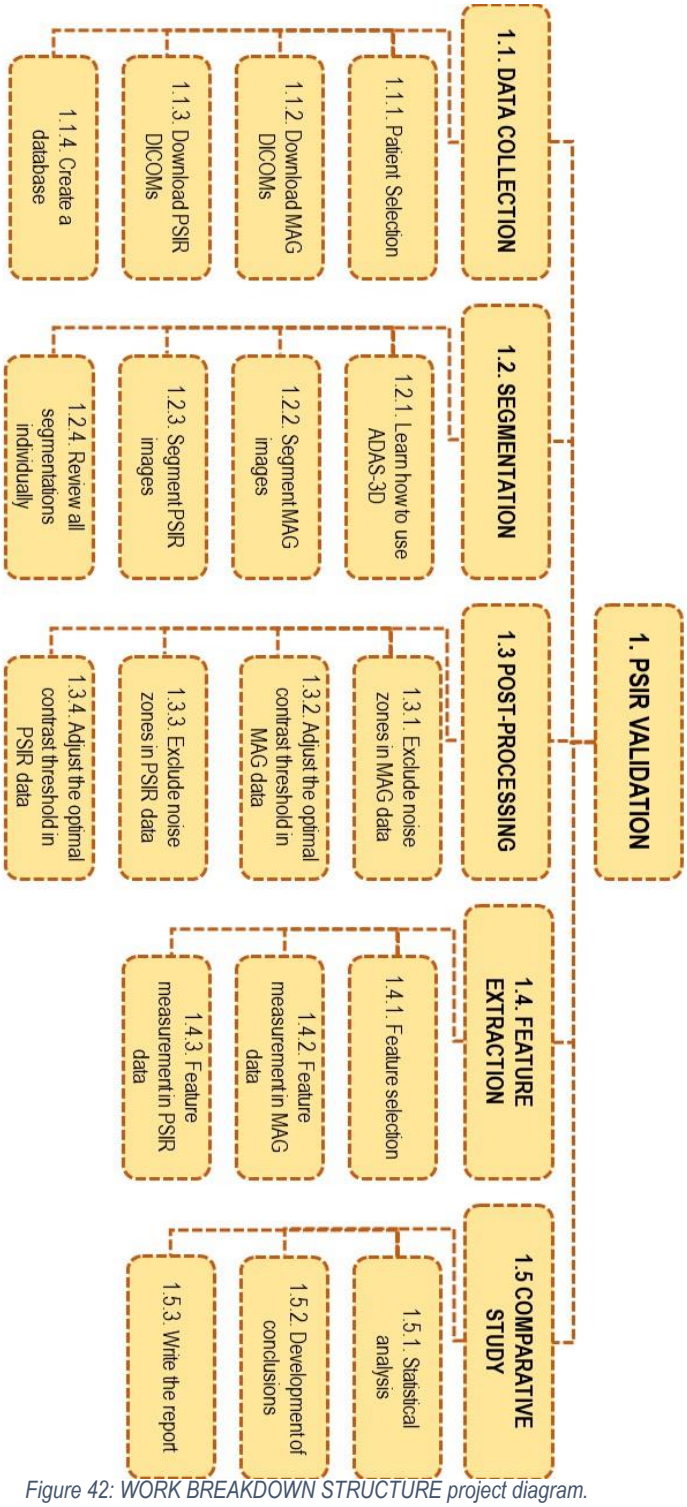

Figure 42: WORK BREAKDOWN STRUCTURE project diagram.

6.2. Task matrix

In the following table we define the tasks to be accomplished for the execution of the project, indicating an estimation of the time expected to be invested in each task, in an optimistic and pessimistic perspective, and the normal time. The unit of measurement of time is days.

DEFINITON	TASK	PREVIOUS TASK	NORMAL TIME μm	OPTIMISTIC TIME μo	PESIMISTIC TIME μp	PROBABILISTIC TIME μj*
Patient Selection	A	-	2	1	4	2,17
Create a database	B	A	2	1	3	2,00
Download MAG DICOMs	C	B	1	1	2	1,17
Download PSIR DICOMs	D	A	1	1	2	1,17
Learn how to use ADAS-3D	E	-	7	4	9	6,83
Segment MAG images	F	C, E	7	4	12	7,33
Segment PSIR images	G	D, E	14	7	16	13,17
Review MAG segmentations individually	H	F	7	3	10	6,83
Review PSIR segmentations individually	I	G	7	3	10	6,83
Exclude noise zones in MAG data	J	H	7	4	10	7,00
Adjust the optimal contrast threshold in MAG data	K	J	7	5	14	7,83
Exclude noise zones in PSIR data	L	I	7	4	10	7,00
Adjust the optimal contrast threshold in PSIR data	M	L	7	5	14	7,83
Feature selection	N	-	2	1	4	2,17
Feature measurement in MAG data	O	K, N	1	1	2	1,17
Feature measurement in PSIR data	P	M, N	1	1	2	1,17
Statistical analysis	Q	O, P	10	7	14	10,17

Development of conclusions	R	Q	3	2	5	3,17
Finish the report	S	R	14	10	16	13,67

Table 7: Matrix of tasks with their order of achievement and their duration time (normal, optimistic, pessimistic and probabilistic.

The probabilistic time is defined in Equation 1.

$$\mu j * = \frac{\mu o + 4\mu m + \mu p}{6}$$

Equation 4: Probabilistic time formula.

The reason why the time dedicated to the segmentation of MAG images is less than the time dedicated to the segmentation of PSIR images is due to the fact that part of the tests taken with MAG have been provided to me already segmented, a fact that means a considerable reduction of work for me.

6.3. CPM/PERT diagram

From the data provided in the task matrix, we can develop the PERT/CPM diagram. In this network diagram we define the connectivity and dependency between tasks, which allows us to find the critical paths. The unit of measurement for the late and early times is days.

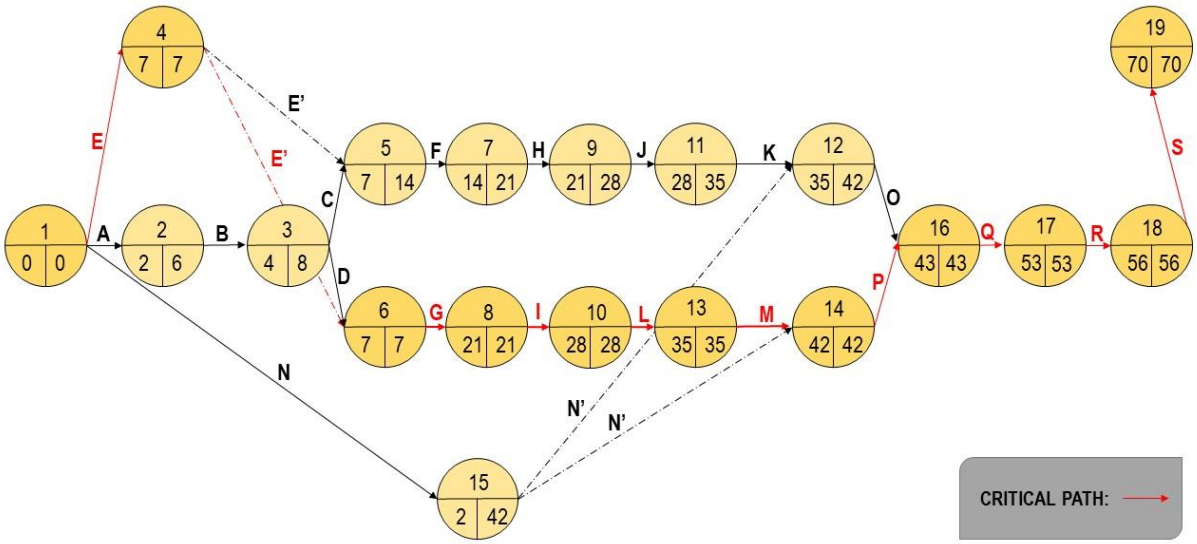

Figure 43: PERT/CPM project diagram.

In red is the critical path of the project, which can trigger a project delay if the included tasks are not completed on time. This path is the one that determines the duration of the project and on which we must exercise more control. Keep in mind that the times are approximate, so an error in the time estimate may trigger a change in the critical path, because the time difference with other paths is not very large.

6.4. GANTT timing

A dedication of approximately 21 hours per week (3 hours per day) is foreseen, and the start date for the execution of the project task is scheduled for September 14, 2021.

To design the GANTT time chart, the following table must be defined, with the scheduled start and end date for each task, as well as its duration. The duration of the tasks is also expressed in days.

DEFINITION	TASK	INITIAL DAY	DURATION	END DAY
Patient Selection	A	20-sep	2	22-sep
Create a database	B	22-sep	2	24-sep
Download MAG DICOMs	C	22-sep	1	23-sep
Download PSIR DICOMs	D	23-sep	1	24-sep
Learn how to use ADAS-3D	E	20-sep	7	27-sep
Segment MAG images	F	27-sep	7	04-oct
Segment PSIR images	G	04-oct	14	18-oct
Review MAG segmentations individually	H	18-oct	7	25-oct
Review PSIR segmentations individually	I	01-nov	7	08-nov
Exclude noise zones in MAG data	J	08-nov	7	15-nov
Adjust the optimal contrast threshold in MAG data	K	15-nov	7	22-nov
Exclude noise zones in PSIR data	L	22-nov	7	29-nov
Adjust the optimal contrast threshold in PSIR data	M	29-nov	7	06-dic
Feature selection	N	06-dic	2	08-dic
Feature measurement in MAG data	O	08-dic	7	15-dic
Feature measurement in PSIR data	P	15-dic	7	22-dic
Statistical analysis	Q	22-dic	10	01-jan
Development of conclusions	R	01-jan	3	04-jan
Finish the report	S	04-jan	14	18-jan

Table 8: Table showing the expected timings for each task.

From this schedule we can have an overview of the scheduled tasks in a visual way. As the person responsible for the development of each task is the same, there are no tasks performed simultaneously. As we can see, the start date is scheduled to be September 14, 2021, and the end of the project is scheduled for January 18, 2021. Thus, after the end there will still be time for writing and revising the report and preparing the oral presentation.

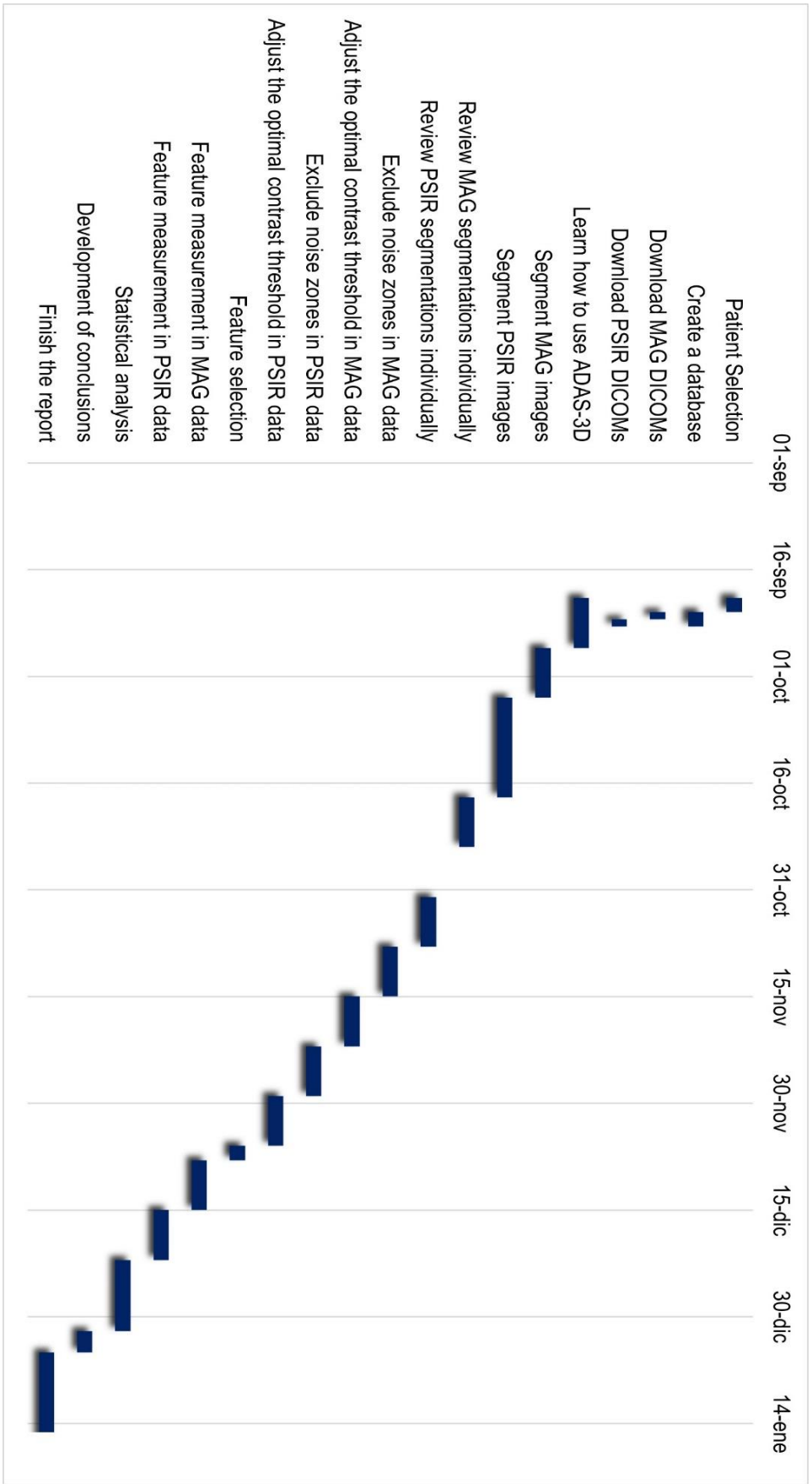

Figure 44: GANTT project diagram.

7. TECHNICAL FEASIBILITY

For the proposed solutions, an analysis has been done to study the situation of the project, through a SWOT matrix of the internal and external characteristics of the work.

	INTERNAL ANALYSIS	*EXTERNAL ANALYSIS*
POSITIVE	STRENGHTS It is a non-invasive technique that does not expose the patient to radiation. Saves time and costs to perform cardiopathological studies. It is an improvement in ablation treatment. Accuracy and safety.	OPPORTUNITIES Support and backup of arrhythmia units in hospitals. Increasing development of cardioresonance imaging technology and software.
NEGATIVE	WEAKNESSES Results are operator dependent (segmentation and processing). Data obtained from patients may be insufficient and therefore inconclusive. Occurrence of noise that alters the signal.	THREATS Lack of standardization in the measurement of values from different trading houses. Development of new alternative technologies.

Table 9: Project SWOT matrix.

First of all, when thinking about the strengths involved in the clarification of this research, we must take into account the advantages that this method of acquiring anatomical images of the heart has over other methods. With respect to x-ray or CT image acquisition, MRI has the benefit of not subjecting the patient to harmful ionizing radiation. Likewise, with respect to the electroanatomical maps performed with catheterization, we can assure that this method is an advantage for the patient's well-being, since it is a non-invasive technique. It is also a more accurate diagnostic study of ischemic heart disease and a great improvement for catheter guidance support in ablation procedures to treat VT.

The main weaknesses of this study are that the results do not depend only on the subject under investigation, the MAG and PSIR sequences, but also on the processing and segmentation given to the images, therefore, the final result may be conditioned. Another major weakness is the limited availability of patient data to perform the experimental test, which may also affect the results. Finally, it should also be noted that the occurrence of noise is a distorting agent.

The main opportunity that this project has is that, since it aims to determine an aspect of the treatment of ablations that directly concerns the arrhythmia units in hospital centers, there would be support from these centers in the research. This possibility could be a great support for the execution of the work. At the same time, the fact that cardioresonance image processing and segmentation technology is currently being developed means that research is of greater interest.

Finally, the main threats to this project are the lack of standardization in the measurement of values from different commercial companies and the fact that the development of new alternative technologies could lead this technique to disuse.

8. ECONOMIC FESEABILITY

First of all, it should be noted that this project does not have a high cost for several reasons. Since this is a research project that does not require the design or development of any prototype and, in addition, since we are working with data and not samples, there is no material cost. Since both the data I need and the equipment necessary to process them are already available at the arrhythmia unit of the Hospital Clínic, where I will carry out the experimental development of my work, the cost is only the amortization of this equipment, since it will not be necessary to make any purchase.

The data selection is provided by the hospital and, therefore, does not involve any expense. The equipment to be used and whose amortization should be taken into account consists of the ADAS-3D segmentation software, the informatics platform used by the Hospital Clínic network to store the diagnostic images of the patients with their relative information (ALMA), the Excel program as a support to obtain the database, a statistical software (SPSS and RStudio) to perform the comparison and a work computer.

	Linear amortization rate (%)	*Commercial price (€)*	*Amortization (€)*
ADAS-3D	33/4 = 8,25	750 approximately	61,875
ALMA	Free	0	0
Excel	33/4 = 8,25	88,28	7,326
SPSS	33/4 = 8,25	21,40	1,765
RStudio	Free for academic institutions	0	0
PC	25/4 = 6,25	1000	62,5
Windows 10	33/4 = 8,25	140	11,5
TOTAL			144,966

Table 10: Table of project amortization quotes.

In the table above, I have calculated the depreciation of the equipment necessary for my research, taking into account the table of straight-line depreciation coefficients determined by the tax agency in Spain.**26** (*Tabla de Coeficientes de Amortización Lineal. - Agencia Tributaria*, n.d.) I have had to divide each value by 4 because these coefficients represent the linear depreciation over one year and I will only use it for 3 months. The maximum depreciation period for this equipment, according to the tax agency, is 10 years and, as the equipment at the Hospital Clínic is fairly new, I have not taken this into account.

Apart from the above mentioned costs, it should be taken into account that the work surface is estimated at about 20€/hour, and as this final degree project is sized for a total of 300 hours, the total cost of the work surface will reach 6.000€. The total cost of the project, considering the hours worked and the amortization of the equipment amounts to **6.145€**.

9. REGULATIONS AND LEGAL ASPECTS

In the development and course of this project, the only stage that requires information on the regulations and legal aspects that concern it, since there is a direct deal with it, is the phase of data selection. Therefore, it must be taken into account that this phase of the study complies with the regulations established in the RGPD (General Data Protection Regulation) and in the LOPDGDD (Organic Law on Data Protection and Guarantee of Digital Rights).

Specifically, compliance with the Data Protection Law must be ensured in clinics and healthcare centers. To this end, the following conditions must be met:

- The data collected must always be relevant and truthful.
- The patient must always be informed and have free access to his or her data.
- Conduct an impact assessment and keep a record of processing activities.
- Appoint a Data Protection Officer.
- Encrypt the data and store them under strict security measures.
- Maintain professional secrecy in all cases.
- In case of transfer of data to third parties, as would be the case of this work, a contract must be signed that establishes the determined and defined use of the transferred data.
- Facilitate the ARCO rights respecting the established deadlines. These rights that the patient has are those of access, rectification, cancellation, opposition, limitation and portability.

When clinical studies are carried out, such as the one in this project, as a general rule, the patient's unequivocal consent must be obtained. In order to have such consent, the patient should be informed that his or her data will be used for research purposes. Another option would be to separate identifying data from medical data, in other words, to anonymize the data so that the patient could not be identified through them.**27** (*REGLAMENTO (UE) 2016/ 679 DEL PARLAMENTO EUROPEO Y DEL CONSEJO - de 27 de Abril de 2016 - Relativo a La Protección de Las Personas Físicas En Lo Que Respecta Al Tratamiento de Datos Personales y a La Libre Circulación de Estos Datos y Por El Que Se Deroga La Directiva 95/ 46/ CE (Reglamento General de Protección de Datos)*, n.d.)

In addition to the data protection law, the company also uses medical diagnostic software, which is considered medical equipment and therefore had to pass ISO 13485 certification, which is the standard for the quality management system applicable to medical devices and medical devices. In this case, all the software I have used has this certification.**28** (*ISO - ISO 13485 — Medical Devices*, n.d.)

10. CONCLUSIONS AND FUTURE LINES

This project has studied the validity of the PSIR magnetic resonance reconstruction sequence for diagnosing and characterizing cases of ischemic ventricular tachycardia.

In order to carry out this work and to enter into context with the object of study, an exhaustive previous investigation of all those aspects related to this sequence has been done, searching for scientific information about ventricular tachycardia of ischemic origin, ventricular ablation, the fundamental operation of magnetic resonance, late gadolinium enhancement, the reconstruction methods to obtain images by magnetic resonance, the existing methodologies to process and represent these images. In addition, in order to have a wider perspective of the project, a study of the historical evolution of this technology and its current market situation has been carried out.

Next, as soon as a sufficient level of theoretical understanding has been achieved, the experimental part of the work has been developed, where we have worked with magnetic resonance images with specific characteristics, coming from patients, in order to obtain the necessary data to develop an analysis that has given an answer to the questions raised at the beginning of the project. In order to assess the degree of satisfaction with the study performed, I proceed to discuss the specific objectives that have been met.

Firstly, it is important to emphasize the achievement in obtaining real and adequate patient data for the development of the project. There were no problems in determining the characteristics of the patients whose ventricular images were the basis for the study. Nor have there been any problems in accessing the information and making the data available, as a total of 30 patients meeting the necessary conditions and with MAG and PSIR samples have been obtained. The knowledge and experience of my tutor has greatly facilitated this task.

It is also valid to affirm that the most labour-intensive stage of the project dealing with the data has been successfully developed, achieving the goal of learning how to segment and process cardioresonance images with ADAS-3D software. For each reconstruction sequence, 21 segmented three-dimensional LV models with interpretative substrate information were obtained. For this purpose, each sample was segmented, processed, discrimination threshold adjusted and rendered.

The stage of parameter extraction and creation of a database with descriptive information of the cases for subsequent analysis of the results has been achieved correctly, although several inconvenient has appeared in this part due to a lack of foresight when structuring the database. As for the selection of parameters, all those provided by the ADAS-3D program and which provide information on the ventricular substrate were taken into account, so that at the end of this part a database with a large number of variables was generated. Moreover, the database was not structured correctly, as the statistical study that was to be performed was not taken into account at the time of completing this database. For this reason, the database had to be restructured in order to carry out the statistical analysis of the data obtained in the SPSS program. Even with the problems that arose, which entailed the additional task of restructuring the database, the objective initially set for this stage was successfully achieved.

The statistical analysis was carried out with the RStudio programme. This part of the project went smoothly, although it required some statistical training to interpret the results. It was divided into two parts: determining the optimal thresholds for PSIR and validating the PSIR sequence by comparing it with MAG. In the first part, statistical indicators (mean, deviation, standard error) were calculated from the thresholds set during the segmentations. Their statistical significance has been demonstrated by applying the student's t-test and the difference between means has been calculated. In general, it has been concluded that, for PSIR images, it is appropriate to increase the thresholds by about 20 points compared to the 40 - 60 range used for MAG images. However, it has been emphasised that each case should be reviewed independently. In the second part, the characterisation of the channels (number and total mass) and the characterisation of the tissue (area of healthy tissue, BZ and core) were analysed. Regarding the channels, it has been concluded that they can measure the total mass with a high degree of accuracy but fail to count them. With regard to tissue type quantification, some positive correlation (overall correlation index = 0.61) and high accuracy (overall measurement error = 0.56) has been demonstrated, with variation depending on the size of the measurement. It has also been shown that PSIR is more accurate in quantifying fibrotic tissue than healthy tissue.

Finally, it is concluded that the validation of the PSIR sequence to determine arrhythmogenic channels depends on two factors. The first is the choice of the variables considered most relevant for the determination of the channels, as some of them show quite different behaviours. The second is the level of similarity considered sufficient to pass validation.

In my view, these results are not sufficient to validate the sequence. The reasons for my conclusion are twofold. The first is that, although the measurement of the masses of the channels is accurate, I consider it a relevant factor to account for them correctly. The second is that, although the identification of ventricular tissue has a high degree of accuracy, I believe that the accuracy in identifying the BZ tissue, which is where the channels are located and where the study is focused, should be higher.

My high demands when validating the PSIR sequence are due to the fact that I attach more clinical value to the accuracy and thoroughness demonstrated up to now by the MAG sequence than to the advantages and improvements demonstrated up to now by the PSIR sequence. Another reason for my requirement is that I consider that technologies with clinical applications directly related to patient health require high acceptability criteria.

10.1 Future Lines of the Project

The field of MRI for medical purposes is therefore a growing area of particular interest to the biomedical sector. Therefore, there is still much to be advanced and studied in this environment, and in particular, for the PSIR reconstruction sequence, which has proven to be a very promising technology.

There are several ways to continue the study and improve the comparative analysis to ensure stronger validation. These new methods should be aimed at eliminating limitations. One of them is to eliminate as many dependent operators as possible to avoid errors that influence the results.

The solution would be to automate as many processes as possible, as there are several phases, such as segmentation or threshold adjustment, that induce errors. On the other hand, it would be interesting to increase the sample size to a minimum of 30 in order to obtain more representative results. It would also be helpful to find out how to obtain more descriptive variables useful for the project (location of channels, shape of channels, severity, for example) and to investigate in more depth how they affect the arrhythmia in order to include them in the data analysis. Finally, it would also be possible to perform a more complex study of the data to obtain more information and eliminate outliers to obtain more accurate statistical results.

Regarding the future prospects of this project, different lines of work can be defined. The most interesting evolution of the project would be, once the PSIR sequence has been validated, to resolve the question of which of the two main reconstruction sequences is the most useful and effective for determining the arrhythmogenic channels in this type of heart disease.

In order to develop this future project, a comparative study between both sequences would be convenient, taking as a reference data obtained by means of an image technique of evidently superior quality, such as electroanatomical maps. This would require a larger amount of data to carry out the study and would entail an undoubtedly greater volume of work.

Lastly, another line of future research that would be of great value to the project would be to test the correct localisation of the channels in the ventricular tissue.

11. BIBLIOGRAPHY

1 Fernández-Armenta, J., Galiano, N. C., Penela, D., & García-Bolao, I. (2013). Actualización en taquicardia ventricular. *Medicine (Spain)*, *11*(39), 2346–2355. https://doi.org/10.1016/S0304-5412(13)70628-0

2 Barrabés, J. A., Bodí, V., Jiménez-Candil, J., & Fernández-Ortiz, A. (2011). Actualización en cardiopatía isquémica. *Revista Espanola de Cardiologia*, *64*(SUPPL. 1), 50–58. https://doi.org/10.1016/S0300-8932(11)70007-0

3 Benito, B., & Josephson, M. E. (2012). Taquicardia ventricular en la enfermedad coronaria. *Revista Espanola de Cardiologia*, *65*(10), 939–955. https://doi.org/10.1016/j.recesp.2012.03.027

4 Berruezo, A., Fernández-Armenta, J., Mont, L., Zeljko, H., Andreu, D., Csaba Herczku, B. ;, Boussy, T., Jose, ;, Tolosana, M., Arbelo, E., & Brugada, J. (2012). *Combined Endocardial and Epicardial Catheter Ablation in Arrhythmogenic Right Ventricular Dysplasia Incorporating Scar Dechanneling Technique*. https://doi.org/10.1161/CIRCEP.110.960740

5 Fernández-Armenta, Juan, Andreu, D., Penela, D., Trucco, E., Cipolletta, L., Arbelo, E., Berne, P., María Tolosana, J., Pedrote, A., Brugada, J., Mont, L., & Berruezo, A. (2014). Sinus rhythm detection of conducting channels and ventricular tachycardia isthmus in arrhythmogenic right ventricular cardiomyopathy. *Heart Rhythm*, *11*(5), 747–754. https://doi.org/10.1016/j.hrthm.2014.02.016

6 Acosta, J., Fernández-Armenta, J., & Berruezo, A. (2016). Ablation of ventricular tachycardia: Indications and results. *Cardiocore*, *51*(3), 99–103. https://doi.org/10.1016/j.carcor.2016.04.002

7 Guandalini, G. S., Liang, J. J., & Marchlinski, F. E. (2019). Ventricular Tachycardia Ablation: Past, Present, and Future Perspectives. *JACC: Clinical Electrophysiology*, *5*(12), 1363–1383. https://doi.org/10.1016/j.jacep.2019.09.015

8 Healthcare, B., Diagnostics, B., Pharmaceuticals, M., Diagnostics, B., Imaging, M., & Billerica, N. (2014). *Gadolinium-Based Contrast Agents : What Does " Single-Dose " Mean Anymore ? 1345*, 1343–1345. https://doi.org/10.1002/jmri.24352

9 Valbuena-lo, S. (2016). *Resonancia magnética cardiovascular en la práctica cardiológica: una guía concisa para la adquisición de imágenes y la interpretación clínica*. *69*(2), 202–210.

10 Young, G. M. B. and I. R. (1999). *Mr Imaging: Clinical Use of the Inversion Recovery Sequence* (p. 13).

11 Chou, S. S., Walker, C. M., & Chung, J. H. (2013). *Ischemic Late Gadolinium Enhancement Ischemic late gadolinium enhancement*. *28*(5), 67–68.

12 Hansen, M. S., & Kellman, P. (2015). Image Reconstruction: An Overview for Clinicians. *J. Magn. Reson. Imaging*, *41*, 573–585. https://doi.org/10.1002/jmri.24687

13 Juan, L. J., Crean, A. M., & Wintersperger, B. J. (2015). Late Gadolinium Enhancement Imaging in Assessment of Myocardial Viability Techniques and Clinical Applications.

Radiologic Clinics of NA, *53*, 397–411. https://doi.org/10.1016/j.rcl.2014.11.004

14 Vogel-claussen, J., Rochitte, C. E., & Wu, K. C. (2006). Delayed Enhance- ment MR Imaging : Utility in Myocardial OBJECTIVES. *RadioGraphics*, *26*(3), 795–811. http://radiographics.rsna.org/content/26/3/795.full

15 Huber, A. M., Schoenberg, S. O., Hayes, C., Spannagl, B., Engelmann, M. G., Franz, W. M., & Reiser, M. F. (2005). *Radiology Imaging in the Detection of*. *4*.

16 Hal, L. O., & Jr, R. W. (1995). *MRI SEGMENTATION: METHODS AND APPLICATIONS*. *13*(3), 343–368.

17 *ADAS 3D LV: Technology*. (n.d.). Retrieved June 3, 2021, from https://www.adas3d.com/en/adas-vt-technology.html

18 Kellman, P., Arai, A. E., Mcveigh, E. R., & Aletras, A. H. (n.d.). *Phase-Sensitive Inversion Recovery for Detecting Myocardial Infarction Using Gadolinium-Delayed Hyperenhancement*. https://doi.org/10.1002/mrm.10051

19 Moran, P. R., Kumar, N. G., Karstaedt, N., & Jackels, S. C. (1986). Tissue contrast enhancement: Image reconstruction algorithm and selection of TI in inversion recovery MRI. In *Magnetic Resonance Imaging* (Vol. 4, Issue 3, pp. 229–235). https://doi.org/10.1016/0730-725X(86)91062-3

20 *Gadolinium-Based Contrast Agents: What Does "Single-Dose" Mean Anymore?* (n.d.). https://doi.org/10.1002/jmri.24352

21 *Patent_PSIR*. (2000). https://patents.google.com/patent/EP0984294B1

22 Ma, J. (2005). *Multislice and Multicoil Phase-Sensitive Inversion-Recovery Imaging*. https://doi.org/10.1002/mrm.20414

23 Hou, P., Hasan, K. M., Sitton, C. W., Wolinsky, J. S., & Narayana, P. A. (n.d.). *Phase-Sensitive T1 Inversion Recovery Imaging: A Time-Efficient Interleaved Technique for Improved Tissue Contrast in Neuroimaging*.

24 Zhuang, X., & Shen, J. (2016). Multi-scale patch and multi-modality atlases for whole heart segmentation of MRI R. *Medical Image Analysis*, *31*, 77–87. https://doi.org/10.1016/j.media.2016.02.006

25 Vanegas, D. I., Álvarez, A., Pava, L. F., Agudelo, J. F., & Martínez, C. (2016). Capítulo 1. Principios básicos del mapeo tridimensional. *Revista Colombiana de Cardiologia*, *23*, 4–16. https://doi.org/10.1016/j.rccar.2016.03.004

26 *Tabla de coeficientes de amortización lineal. - Agencia Tributaria*. (n.d.). Retrieved June 6, 2021, from https://www.agenciatributaria.es/AEAT.internet/Inicio/_Segmentos_/Empresas_y_profesionales/Empresas/Impuesto_sobre_Sociedades/Periodos_impositivos_a_partir_de_1_1_2015/Base_imponible/Amortizacion/Tabla_de_coeficientes_de_amortizacion_lineal_.shtml

27 *REGLAMENTO (UE) 2016/ 679 DEL PARLAMENTO EUROPEO Y DEL CONSEJO - de 27 de abril de 2016 - relativo a la protección de las personas físicas en lo que respecta al tratamiento de datos personales y a la libre circulación de estos datos y*

por el que se deroga la Directiva 95/ 46/ CE (Reglamento general de protección de datos). (n.d.).

28 *ISO - ISO 13485 — Medical devices*. (n.d.). Retrieved June 6, 2021, from https://www.iso.org/iso-13485-medical-devices.html

29 *Gaztañaga, L., Marchlinski, F. E., & Betensky, B. P. (2012). Mecanismos de las arritmias cardiacas. Revista Espanola de Cardiologia, 65(2), 174–185. https://doi.org/10.1016/j.recesp.2011.09.018*